UNIVERSITY OF OKLAHOMA

GRADUATE COLLEGE

RADAR ANALYSIS OF THE PHYSICS OF EXTREME RAINFALL EVENTS

A THESIS

SUBMITTED TO THE GRADUATE FACULTY

in partial fulfillment of the requirements for the

Degree of

MASTER OF SCIENCE IN METEOROLOGY

By

RYAN BUNKER
Norman, Oklahoma
2020

RADAR ANALYSIS OF THE PHYSICS OF EXTREME RAINFALL EVENTS

A THESIS APPROVED FOR THE
SCHOOL OF METEOROLOGY

BY THE COMMITTEE CONSISTING OF

Dr. Cameron R. Homeyer, Chair

Dr. Jeffrey B. Basara

Dr. Elinor R. Martin

Acknowledgments

This work in this thesis could not be completed alone. The author would like to thank the thesis committee for their time, ideas, and assistance throughout the research process. I would like to thank Dr. Homeyer for his support with the research, his mentorship, and his time spent editing all the work that has been done. Furthermore, I would like to extend an additional thank you to Ty Dickinson and Melanie Schroers for providing figures and additional ideas in the analyses of this work. Additionally, my family and friends deserve acknowledgement for their support throughout this process. The author thanks other members of the PRES^{2}iP research group and the Convection, Chemistry, and Climate research group. This work is supported by the National Science Foundation under their Prediction of and Resilience against Extreme Events (PREEVENTS) program (Grant #1663840).

Table of Contents

List of Tables

List of Figures

Abstract

Extreme precipitation events pose a threat to life, property, and economic growth throughout the United States and across the world. Although extensive research has focused on improving understanding of extreme precipitation at short space and time scales, there is still much that needs to be understood on the subseasonal to seasonal (S2S) timescale. This thesis uses a database of observed S2S extreme precipitation events in the United States and high-resolution ground-based radar observations to identify the leading source of precipitation, either convective or stratiform, and how it varies based on event type (location, dynamics, season, etc.). S2S precipitation events are defined as 2-week precipitation accumulations that exceed the 95th percentile accumulation for a given location and time period, along with exceedance of percentile thresholds and spatial extent criteria. A 3-D radar echo classification algorithm was used to objectively stratify precipitation into convective and stratiform components. Using these identified events, atmospheric variables from reanalysis (i.e., geopotential height, winds, 850 hPa relative humidity, 850 hPa temperature, mean sea level pressure, and precipitable water) are used to gain an understanding of the evolution of the atmospheric state during the precipitation events. Common synoptic patterns seen during these events include troughing upstream of the precipitating region, deep moisture transport into the region, and a synoptic-scale boundary in close proximity to precipitation. For example, the Northern Plains, Great Lakes, and Northeast events were all characterized as mid-latitude environments; whereas the Southern Plains had 3 mid-latitude events and 3 tropical events, and the Southeast had 4 mid-latitude events and 2 tropical events. The primary differentiation among these different environments were the upper-level forcing (or lack thereof for tropical environments) and baroclinic boundaries associated with extratropical cyclones. Seasonally, tropical environments and associated convective dominance took place in the summer to early fall across the Southern Plains and

Southeast. Regions that were more poleward (i.e., Northern Plains, Great Lakes, and Northeast) were predominately stratiform dominant, except for a few events in the summer where convection was dominant. All together, these results represent a progressive step forward in helping understand S2S events and their characteristics on a regional scale.

Chapter 1

Introduction

Extreme precipitation events are a natural disaster in the contiguous United States (CONUS) that pose a threat to life, property, and the economy. Although flooding can emerge from multiple different origins (i.e., snow melt, river flooding, coastal flooding, etc.), extreme precipitation contributes significantly to this problem. Floods were the second deadliest United States weather-related hazard in 2018, behind heat-related deaths. Moreover, floods were the third costliest weather-related hazard that year at just over $1.6 billion, trailing only behind tropical cyclones and fire weather (National Weather Service, 2018a). The U.S Natural Hazard Statistics showed that from 1989-2018, floods were the second deadliest weather-related hazard, trailing behind heat (National Weather Service, 2018b). These devastating hazards and associated losses reiterate the need for improved understanding of these extreme precipitation events. Although extensive research has focused on improving understanding of extreme precipitation at short space and time scales, there is still much that needs to be understood at the subseasonal to seasonal (S2S) timescale. To help the lack of understanding at this timescale, this study is a part of the Prediction of Rainfall Extremes at Subseasonal to Seasonal Periods (PRES^{2}IP) project, funded through the National Science Foundation (NSF) Prediction of and Resilience against Extreme Events (PREEVENTS) program. The primary goal of the PRES^{2}IP project is to understand the primary forcings and large-scale dynamics of extreme precipitation events on the S2S timescale. These S2S extreme precipitation events tend to have more widespread impacts than daily or sub-daily precipitation events owing to the spatial scale and longevity of each event. Flash flooding events, which are on a time scale of hours to a day, are predominately caused by convective precipitation. On the

S2S timescale, however, the primary source of precipitation is not well-understood. To understand the nature of these extreme precipitation events, it is important to identify the leading source of precipitation, either convective or stratiform.

1.1 Socioeconomic Impacts of Extreme Precipitation Events

Flooding events are naturally occurring events that depend on a multitude of factors such as rainfall rates and amounts, topography of a given region, land use of the region, and antecedent moisture conditions (Funk, 2006). Extreme precipitation events can be destructive to a society when people are located in vulnerable locations that are more susceptible to flooding. Ashley and Ashley (2008) studied a 47-yr period and found that there were a total of 4586 reported fatalities from flooding across the CONUS. In addition, they found that people between the ages of 10 and 29, and greater than 60 years old are more vulnerable to floods.

A specific example of an extreme precipitation event occurred in Colorado during September 2013 when multiple days of rainfall led to historical flooding across the area. In fact, a 24-hr rainfall record was set for Boulder when 9.08 inches fell between 0000 UTC 12 September and 0000 UTC 13 September 2013 (National Weather Service, 2013). This event was responsible for nearly $4 billion in damages, 9 fatalities, over 19,000 persons evacuated, and multiple homes, businesses, and roads/infrastructures destroyed. In Louisville, Kentucky on 1 March 1997, a 24-h rainfall record was obtained by the NWS Warning Forecast Office (WFO) at 10.48 inches. During this extreme event, approximately $200 million in damages occurred in the Louisville metro area, along with two interstate highways closed, and tens of thousands of people evacuated from their homes (National Weather Service, 1997).

1.2 Short Duration and Long Duration Precipitation Events

Per the American Meteorological Society, a flash flood is caused by a rapid increase in the water level in relatively small areas that occurs within minutes to hours as the result of intense rainfall, ice jams, or levee and dam failures (American Meteorological Society, 2017). Short duration rainfall events are often more hazardous than slower and longer duration floods because of the difficulty in providing warning and emergency response (Ahern et al., 2005). Maddox et al. (1979) was the first to examine the atmospheric patterns associated with flash flood events across the CONUS. This study identified four characteristic patterns that were common among 151 flash flood events. This study concluded that the heavy rains were produced by convective storms, high surface dewpoints, high moisture content throughout the tropospheric layer, and vertical wind shear that was weak to moderate throughout the cloud depth. Several studies (e.g., Brooks and Stensrud, 2000; Schumacher and Johnson, 2006; Dougherty and Rasmussen, 2019; Moore et al., 2015) have looked at climatologies of extreme and flash flood events in the U.S. and found that a majority of these events occur in the warm season. Moore et al. (2015) analyzed extreme precipitation events in the southeastern United States (SEUS) and found that these events occur more frequently in the western portion of the SEUS during the cold season and in the eastern portion during the warm season. Without the influence of tropical cyclones, however, 24-hour extreme precipitation events involved more thermodynamic influences in the warm season, whereas the cold season was influenced by more dynamical contributions (i.e., integrated water vapor transport and rising motion).

On a similar timescale but a broader spatial scale, other studies assessed characteristics of regional extreme precipitation events (e.g., Konrad, 1997; Hitchens et al., 2012; Moore et al., 2012; Stevenson and Schumacher, 2014; Moore et al., 2015). Konrad (1997) examined the characteristic synoptic-scale features associated with heavy

rainfall events during the warm season across the southeastern United States and found five distinct patterns. In four of the five characteristic patterns, heavy rainfall is associated with high levels of moisture at 700-mb. In addition, ridging associated with 850-mb warm air advection was also a key component to heavy rainfall across the southeast United States. Hitchens et al. (2012) used the National Centers for Environmental Prediction (NCEP) stage-II hourly precipitation dataset to explore extreme precipitation across the midwestern United States. This study found that the majority of the events occurred during the summer months, and a drop in frequency between summer and fall. Moore et al. (2012) investigated the physical processes that resulted in devastating flash flooding and prolonged heavy rainfall across western and central Tennessee and Kentucky. The primary support to the longevity of this event was a consistent corridor of deep moisture aided by a strong southerly low-level jet (LLJ) that was positioned between lee troughing over the eastern Mexico coast and a broad, ridge over the southeastern United States.

Certain case studies have aimed to improve the predictability and understanding of key features associated with extreme rainfall events (e.g., Marciano and Lackmann, 2017; Schroeder et al., 2016). Marciano and Lackmann (2017) looked at the excessive rainfall associated with Hurricane Joaquin and found that the diabatic outflow from the hurricane slowed the eastward progression of an upper-level trough. In turn, this provided enhancement of the jet streak and allowed for excessive moisture transport into the region where the flooding event occurred. Schroeder et al. (2016) used archived sounding data and climatological precipitable water (PW) distributions to examine multiple urban flooding events from 1977-2014. A major finding in this study was that these locally heavy precipitation events are characterized by extremely anomalous PW values, with a majority of the events exceeding the 99^{th} percentile. With a similar framework, but a different timescale, Flanagan et al. (2018) looked at atmospheric patterns associated with pluvial years. This study defined a subregion

to be a pluvial year if the calendar-year total precipitation is 10% greater than the climatological annual total precipitation for that subregion. Pluvial patterns across the southern Great Plains (SGP) showed negative height anomalies over the southwestern United States while the northern Great Plains (NGP) were represented by anomalously lower heights in the northwest United States. A key driver for the extreme rainfall events during these pluvial years was an east-west height gradient and strong moisture fluxes that were oriented poleward. Schubert et al. (2008) examined seasonal precipitation in the Great Plains using an ensemble of century-long atmospheric general circulation model (AGCM) output and found that pluvial years were more predictable than drought years. In fact, during the warm season the role of the Atlantic sea surface temperatures (SSTs) acts to force change in the Bermuda high and allow for low-level moisture advection into the region. These studies established an understanding of daily or even sub-weekly extreme precipitation, but a similar understanding of events at the S2S timescale is an emerging focus.

1.3 Convective and Stratiform Components and Their Impacts

Most precipitation systems can be decomposed into two dynamically and microphysically unique modes, convective and stratiform (e.g., Houghton, 1968; Battan, 1973; Anagnostou, 2004; Morrison et al., 2009), though the distinction may not always be evident in observations. One of the main ways to physically differentiate between these two modes is based on the magnitude of the in-cloud vertical air motions (Steiner et al., 1995). From a thermodynamic perspective, the vertical distribution of diabatic heating is distinctly different in convective and stratiform regions (Houze, 1982, 1989; Johnson, 1984). Not only is it important to distinguish between these modes from a thermodynamic standpoint, it is also important to distinguish between their differing precipitation growth mechanisms (Houghton, 1968). Atlas and Ulbrich (2006) demonstrated the necessity to characterize the physical and dynamic nature of

rain storms by using remote sensing for more precise rainfall estimates. The studies above enforce the need to continue to study these precipitation modes in order to better understand their relative contributions to extreme events.

Another way to distinguish between convective and stratiform precipitation is through interpretation or radar reflectivity. Many avenues of research have followed this path to evaluate microphysical differences between convective and stratiform precipitation (e.g., Steiner et al., 1995; Chen et al., 2019; Yang et al., 2019). Other studies have utilized radar observations in order to improve rainfall estimations (Chandrasekar et al., 1993; Austin, 1987; Kirsch et al., 2019) and rainfall rate calculations (Marshall and Palmer, 1948; Ryzhkov et al., 2005; Giangrande and Ryzhkov, 2008; Ryzhkov et al., 2014). Marshall and Palmer (1948) established the conventional rainfall rate calculation by relating reflectivity factor (Z) and rainfall rate (R) using a power law distribution. This research has motivated countless other radar-based rainfall studies. Dual Polarization (Dual Pol), which adds vertical polarization to the traditional horizontally polarized wave, can help to accurately discern the physics of the radar return. In turn, this allows better discrimination between precipitation types (i.e., rain, snow, and hail). Chandrasekar et al. (1993) combined horizontal reflectivity factor (R_{ZH}), differential reflectivity (R_{DR}), and specific differential propagation phase (R_{DP}) to derive the best estimate of rainfall using multiparameter radars. This study found that using R_{ZH} is best for light rain, and a combination of R_{DR} and R_{DP} for moderate and heavy rainfall rates. One of the primary advantages of a Dual Pol radar is the improvement of quantitative precipitation estimation (QPE) because a polarimetric radar is capable of measuring multiple variables from two orthogonally polarized radar beams. Ryzhkov et al. (2005) used Z, differential reflectivity(Z_{DR}), and specific differential phase (K_{DP}) to create a rainfall algorithm for rainfall estimation. By using this algorithm, the root mean square (rms) error of

hourly rain estimates were reduced by 3.7 times for areal rainfall measurements when compared to conventional nonpolarimetric relations.

Comparing fractions of convective and stratiform precipitation is important for climatological studies estimating the heating of the atmosphere and the precipitation contributed by each source. Steiner and Houze (1997) examined the monthly convective rain fraction to variations of the same Z-R relationship used in radar-derived rainfall estimation. This study found a large range of ambiguity for convective rain fractions which ranged from 30% to 80%, depending on the choice of Z-R parameters. In contrast, the convective rain fraction in Melbourne, Florida from this study ranged from 80% to 100%, likely owing to dominance of precipitation from sea-breeze-triggered, multicellular storms around that region. Tao et al. (2010) investigated the relationship between surface rainfall, rainfall intensity, and its associated stratiform amount by using the precipitation dataset from Tropical Rainfall Measurement Mission (TRMM) Precipitation Radar (PR) for the global tropics and subtropics. The results from this study showed that moderate-high stratiform fractions are associated with light rain intensities, whereas convective fractions are associated with higher intensities, but are skewed toward weaker rain rates. Schumacher and Houze (2003) also used TRMM PR to explore stratiform rainfall in the tropics and found that stratiform rain accounts for 40% of the total rainfall. The sensitivities of convective and stratiform fractions could differ in mid latitudes and even on a regional basis. The aforementioned studies above, along with a knowledge gap in the S2S timescale create a pathway for exploration into convective and stratiform sensitivities across the CONUS using high spatial and temporal resolution observations.

Challenges, variations, and limitations all arise when using radar for rain rate calculations. Heavy stratiform rain is often misclassified as convective, and precipitation along the perimeter of convective cores is often misclassified as stratiform (Biggerstaff

and Listemaa, 2000). Uncertainties in Z-R relationships are present for estimated extremes, or the presence of hail or snow when rain is expected (Austin, 1987; Hasan et al., 2014; Seed et al., 2007). Limitations and uncertainties associated with single polarization radars for Z-R relationships include radar miscalibration, attenuation, ground clutter, beam blockage, variability of the Z-R relation, range effects, vertical variability of the precipitation system, and vertical air motion and precipitation drift (Villarini and Krajewski, 2010). While Dual Pol can provide better estimates of rainfall when compared to single Pol for a diverse range of storm types, Dual Pol radars are not consistent for all storms or radars (Cunha et al., 2013). Specifically, Cunha et al. (2013) studied three significant rainfall events in the Kansas City, MO and found that Dual Pol rainfall estimation improvements depend on the range-dependent sampling of the vertical structure of the storms and the associated hydrometeor type.

1.4 The Relationship Between Rainfall Extremes and Climate Change

As previously mentioned above, extreme rainfall and associated flash flooding are one of the most costly and dangerous natural hazards in the world. Extreme daily rainfall frequency and/or intensity has increased over multiple continents throughout the 20th century (Alexander et al., 2006). The potential for the intensity and frequency of extreme rainfall to increase with anthropogenic climate change is of considerable societal concern. Min et al. (2011) was one of the first studies to detect human influence on daily extreme rainfall intensification. In addition, Coumou and Rahmstorf (2012) studied extreme weather events across the world from 2000 to 2011 and found that precipitation extremes will greatly increase in a warming climate because warmer air is capable of holding more moisture. In addition, increased moisture content owing to warmer temperatures can foster more latent energy to drive storms. Trenberth et al. (2003) discussed the characteristics of precipitation under

a changing climate and found that frequencies of precipitation events will decrease, but intensities of precipitation will increase. This is due in part to the increase of precipitable water (PWAT) below 500 mb over the Western Hemisphere north of the equator by about 5% decade^{-}1 (Ross and Elliott, 1996). On a more narrow scale, Westra et al. (2014) looked at subdaily extreme rainfall intensification due to anthropogenic climate change and described the understanding of atmospheric temperature and extreme rainfall intensity. From a physical standpoint, atmospheric temperature strongly affects the intensity of extreme rainfall because the amount of water vapor that can exist in the air increases with increasing temperature and thus, more moisture availability to rainfall events. The atmosphere's capacity to contain water vapor is defined by the Clausius-Clapeyron (CC) equation which expresses the relationship between air's water capacity and its temperature. The CC relationship, considering the surface with a pressure of 10^5Pa at typical surface temperatures, increases at roughly 7% per degree celsius (C) from 0-24°C and about 6% per degree above 24°C (Westra et al., 2014). In fact, Westra et al. (2014) used a Clausius-Clapeyron (CC) scaling method to help build a theoretical basis for extreme rainfall and found that the intensity of hourly or sub-hourly extreme rainfall is more sensitive to local temperature change compared to daily-scale rainfall.

From a modeling standpoint, daily and even longer temporal outputs from general circulation models (GCMs) suggest that extreme rainfall intensities will increase in the mid latitudes with a warming climate (Meehl et al., 2007). Kunkel et al. (2013) showed that there is clear evidence for future increases in the probable maximum precipitation on a daily temporal scale for the CONUS using Coupled Model Intercomparison Project phase 5 (CMIP5) GCMs. In addition, magnitudes of water vapor changes follow temperature changes similar to that from the CC relationship. Studies using Expert Team on Climate Change Detection and Indices (ETCCDI) have indicated large-scale statistically significant increases in extreme rainfall into the future

(Sillmann et al., 2013). The aforementioned studies help explain the potential for future increases in rainfall intensities and/or frequencies with a warming climate. The goal of this study is to fill the knowledge gap of extreme precipitation within the S2S timescale by understanding the source of precipitation, either convective or stratiform. Primary forcings and large-scale drivers of these events will also be an area of focus in order to understand the environments associated with extreme precipitation events.

Chapter 2

Data and Methods

2.1 Data

All radar data used in this study are from the Next Generation Weather Radar (NEXRAD) Weather Surveillance Radar-1988 Doppler (WSR-88D) network (Crum and Alberty, 1993) and the archived data were extracted from Amazon Web services (AWS). The archives included three-dimensional data from each radar system (level 2 data), and were provided on a spherical grid (azimuth, elevation, and range) from the origin of each radar location. Observations from each radar were processed using the Gridded NEXRAD WSR-88D Radar (Gridrad) software and are binned with temporal resolution of 5-min intervals, latitude-longitude grid spacing of 0.02° (2 km), and a 0.5 to 1-km spacing in the vertical. During the binning process, a Gaussian function is used to weight each individual radar observation out to 300 km in range within a 5-min time interval centered on the analysis time. The minimal detectable signal at a 300 km range is 7.5 dBZ; however, the minimum reflectivity threshold for GridRad data is 0 dBZ.

All precipitation data are from the Parameter Regression on Independent Slopes Model (PRISM), which have daily precipitation data with a 4-km resolution from 1981 to present (Daly et al., 2000; PRISM Climate Group). Atmospheric variables from Modern-Era Retrospective Analysis for Research and Applications version 2 (MERRA-2) daily data with a 0.625° x 0.5° horizontal grid are used to evaluate the synoptic features associated with each S2S event (Gelaro et al., 2017). Variables include geopotential heights, wind barbs (kt), 850 hPa relative humidity (RH), 850 hPa temperature, mean sea level pressure (MSLP), and precipitable water (PWAT). Each variable is produced at 3-hour increments. For RH, any value that is greater

than 80% will be considered "high". For PWAT, any value greater than 40 mm in the SP, SE, and GL will be considered "high", and any value greater than 30 mm in the NP and NE will be considered "high". These regional thresholds were based off the Storm Prediction Center's (SPC) sounding climatology page (Storm Prediction Center (SPC)). SPC's climatology page has a 91-day moving average for all of the sounding locations across the CONUS. Here, the 90^{th} percentile moving average was chosen as a good threshold to identify maximum PWAT values during each event. Considering most of the events in this study took place during late spring-summer, the aforementioned regional thresholds reflect this time period. It should be noted that this is location-dependent; that being said, the subjective threshold still holds a good representation of the broader region. Archived surface analyses with observations were created at a 3-hour temporal resolution, were used from the Weather Prediction Center (WPC) (Weather Prediction Center, 2020). Surface analysis observations include temperature and dew point temperature (in F), wind (kt), sea-level pressure, and surface fronts and boundaries.

2.2 Methods

2.2.1 Extreme Event Definition

S2S events used in this study came from a database created by Jennrich et al. (2020), and were found based on an algorithm using a 14-day sliding window from 1 January 1981 to 31 December 2010. They chose the 95^{th} percentile of the distribution to define extreme precipitation at a given location and divided the CONUS into six regions in order to compare and contrast characteristic patterns associated with S2S extreme precipitation events (Figure 2.1 in Jennrich et al. (2020)). In this study, however, the Great Plains (GP) is further divided into two sub-regions, Northern Plains (NP) and Southern Plains (SP) in order to better delineate between the two regions. In addition, the Mountain West (MW) and West Coast (WC) will not be

used in this study owing to poor radar coverage in these mountainous areas (Westrick et al., 1999).

Within a regional framework, four criteria are used to define each 14-day extreme precipitation event. Firstly, the total area rainfall exceeding the 95^{th} percentile of the 14-day precipitation must be above a threshold (Table 1 in Jennrich et al. (2020)). Next, two exclusionary criteria were set for these events; area-averaged precipitation must exceed 10 mm day^{-1} for 5 of the total 14-day sliding window, and the heaviest rainfall day and surrounding two days must not exceed 50% of the event precipitation. Finally, if any of the 14-day events are overlapping with another events' window, the 14-day event with the greatest cumulative precipitation is chosen. Events were created from these criteria and were characterized by region. During 2008, the National Oceanic and Atmospheric Administration (NOAA) upgraded the WSR-88D radars to produce increased spatial resolution data, or in other words, Super Resolution (National Weather Service, 2017). In addition, radar data is routinely available from 2006-present. Because of this, events that were selected for this study were all after 2008, to avoid impacts of varying data quality/resolution in the analyses (i.e., comparing radar data from before 2008 and after 2008). In total, there are 27 cases in this study; 6 in the SP, 6 in the Southeast (SE), 5 in the NP, 5 in the Great Lakes (GL), and 5 in the Northeast (NE). For some regions, these were all of the events available since 2008, and preference was given to the most recent events in regions where there were more than 5 events.

Fig. 2.1 shows an example of the total PRISM precipitation from one of the cases that took place in the SP from April 26, 2009 to May 09, 2009 (hereafter SP20090426). The black contours represent the grid points within the regional domain that are considered extreme as previously defined from Jennrich et al. (2020). In subsequent chapters and sections of this thesis, plots will be shown like Fig. 2.1, but will only include precipitation in regions where the grid points are labeled as extreme.

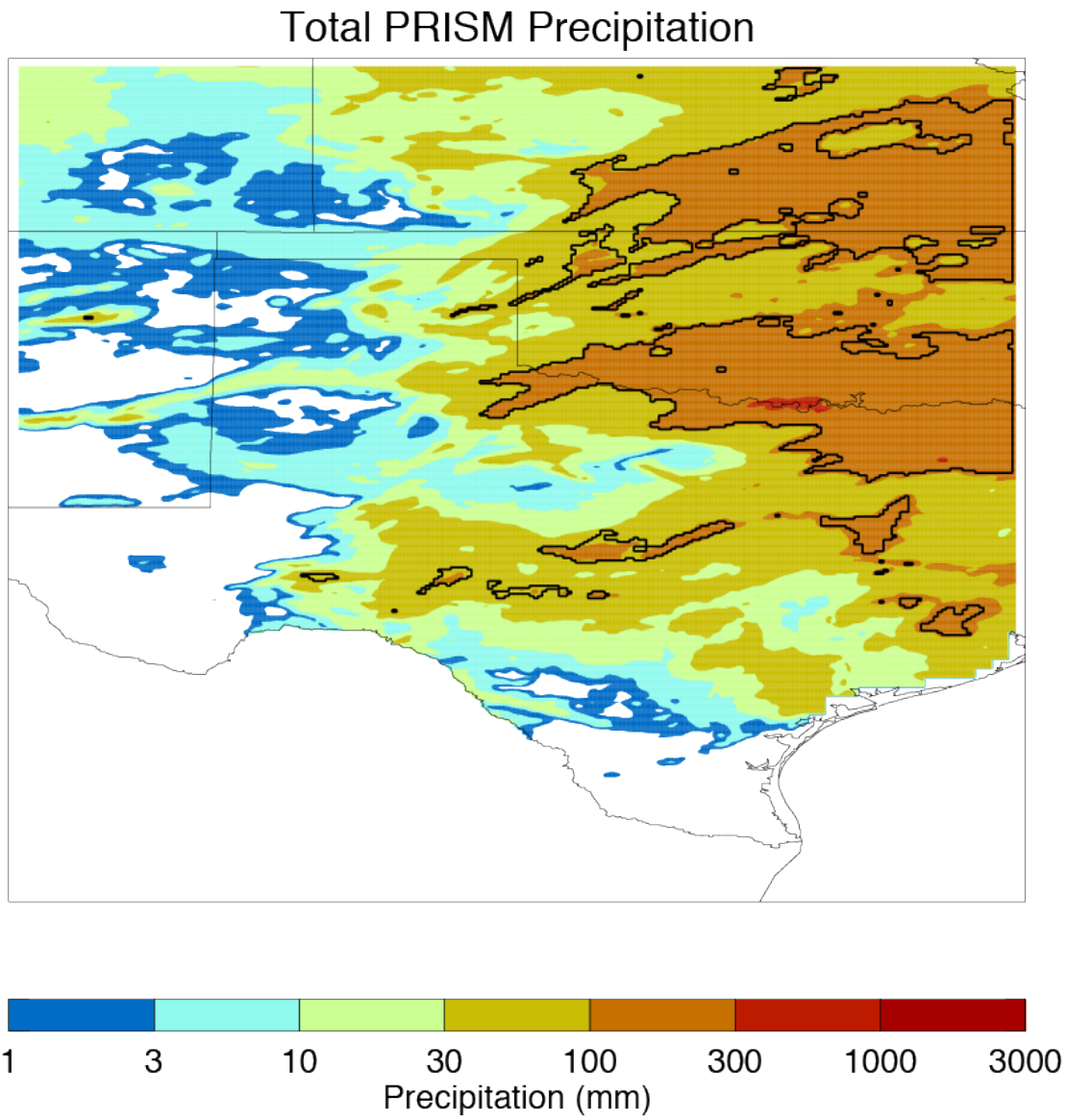

Figure 2.1: Total precipitation (mm) from PRISM for a case in the SP from April 26, 2009 to May 09, 2009. Areas that are labeled as extreme are delineated by black contours.

2.2.2 Radar-Based Rainfall Characterization

Radar utilization for convective/stratiform separation has been well-documented over the years (Steiner et al., 1995; Biggerstaff and Listemaa, 2000; Feng et al., 2011; Powell et al., 2016). For example, Steiner et al. (1995) used a three-step procedure

for identifying convective precipitation. First, any grid point within the radar reflectivity field that exceeded 40 dBZ is automatically labeled as convection. Second, a threshold based on the average background intensity field is used to see if any grid points near the convective maximum should be labeled as convective. Third, for any grid point that is labeled as convective from the first 2 criteria, all surrounding grid points within an intensity-dependent radius, are also labeled as convective. Biggerstaff and Listemaa (2000) built upon the commonly used Steiner et al. (1995) method by computing the vertical lapse rate of Z_H in the 3-km layer above the Z_H column-maximum value in order to improve the classification of heavy stratiform rain (originally classified as convective), and the periphery of convective cores (originally classified as stratiform). These studies have incorporated some information about the vertical structure of the storm, and their primary classification between convective and stratiform precipitation is completed using a single low-altitude threshold of Z_H. In particular, this threshold is disadvantageous because it does not account for the full vertical column within a storm. One study in particular that leverages the three-dimensional reflectivity field to provide confident stratiform/convection type for a given echo is that outlining the Storm Labeling in Three Dimensions (SL3D) algorithm (Starzec et al., 2017). SL3D is a storm classification algorithm that separates radar echo into five components: convection, convective updraft, precipitating stratiform, nonprecipitating stratiform, and ice-only anvil. In this study, SL3D was able to identify larger regions of convection (often misclassified) amongst several cases of varying complexity, intensity, and regionality. The methodology in Starzec et al. (2017) will be the methodology used in this study in order to differentiate between convective and stratiform precipitation.

2.2.3 Sensitivity Tests and Final Analysis Approach

Using a radar-based approach for precipitation estimates and characterization has limitations and these limitations have been well-documented by previous research. Limitations such as the microphysical differences between stratiform and convective precipitation (Houghton, 1968). Houghton (1968) found that the microphysical differences lie in the magnitude of in-cloud vertical motions and the timescale of the precipitation growth processes, which ultimately lead to biases if a single Z-R relationship is used for convective and stratiform precipitation. If the differences in vertical motion within the cloud are not accounted for, this will lead to biases in rainfall rates. Another limitation is data availability and gaps in the NEXRAD WSR-88D network. Westrick et al. (1999) found that as a result of terrain blockage, shallow precipitation, and low freezing levels, only one-fourth to one-third of the land surface across the MW and WC have sufficient radar coverage for precipitation estimation. Miscalibration is another key limitation that affects QPE. For example, Smith et al. (1996) found that on average, the Tulsa, Oklahoma (KINX) radar rainfall estimates were 30% greater than by the Oklahoma City, Oklahoma (KTLX) in the overlapping area due to miscalibration. Smith et al. (2000) found similar results when the bias in rainfall estimation over the Houston, Texas (KHGX) radar and attributed the biases to miscalibration and drop size distribution (DSD). Brightband contamination, which is a Z_H maximum occurring near/in the melting layer in stratiform precipitation, can lead to serious radar-based overestimates in accumulated surface rainfall (Biggerstaff and Listemaa, 2000; Gourley and Calvert, 2003). These limitations all impact the rain totals/rates considerably, however, it is not clear what the sensitivity in convective/stratiform rain fraction is. This study aims to use the fractions of convection and stratiform to get a better idea of the dominating source of precipitation by region.

There are numerous rain-rate relationships that can be used in order to identify the fractions of each source of precipitation. The NEXRAD upgrade to dual-polarization,

many studies have aimed at producing more accurate estimates of rainfall using dual-polarization variables. As mentioned in Section 1.3, Ryzhkov et al. (2005, 2014) (hereafter called the polarimetric relationship and specific attenuation relationship, respectively) used different polarimetric variables to gain a better understanding of rainfall estimates. These studies used dual-polarization variables because Z-R relationships are typically biased high for weak rain rates, and low for high rain rates where microphysical diversity is large for radar measurements. There are, however, well-established Z-R relationships for the U.S. that are commonly applied for research and nowcasting applications with NEXRAD WSR-88D data (Grams et al., 2014). The ideal stratiform Z-R relationship is a hybrid between warm stratiform rain and cool stratiform rain relationships based on the reflectivity thresholds in Table 1 of Warning Decision Training Division (WDTD) (2014). Ideal convective Z-R relationships comprise a tropical relationship and a mid-latitude relationship (Table 2 in Warning Decision Training Division (WDTD) (2014)) for which knowledge of the meteorological environment informs their use for a given event. These well-calibrated Z-R relationships are used in this study to determine convective/stratiform rain fractions.

Radar data acquisition over a large spatiotemporal scale is computationally expensive. For this reason, sensitivities of retrieved rain fractions to data frequency were evaluated at 5-minute, 10-minute, 15-minute, 20-minute, and 30 minute increments. Fig. 2.2 illustrates the convective fraction of the same case when the time increment is adjusted. In Fig. 2.2a-c, there is little-to-no sensitivity in the data among the time intervals. When the time interval is every 20 minutes (i.e., Fig. 2.2d), however, the patterns begin to become more coarse and variable. At 20 and 30 minutes intervals, too much of the signal gleaned from higher temporal sampling is missed in a 14-day event. Thus, it was determined that using 15-minute data for each 14-day case would not adversely affect the resulting fractions but increase efficiency.

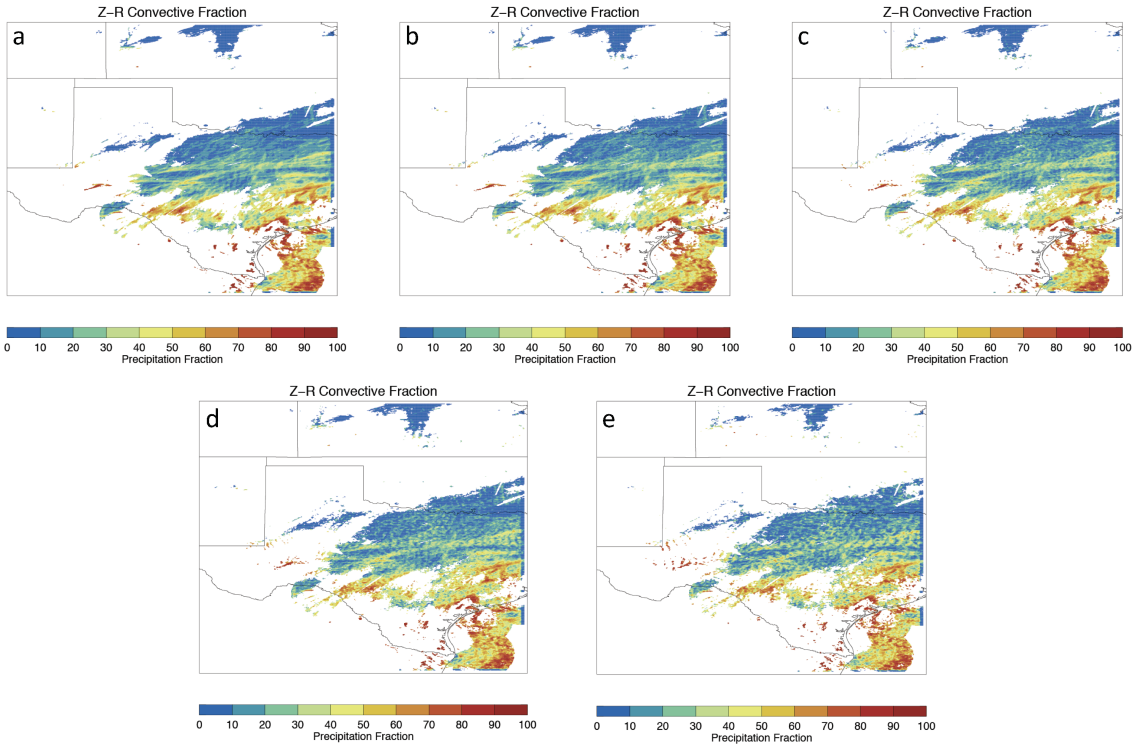

Figure 2.2: Total convective fraction with time sensitivities of a.) 5 minutes b.) 10 minutes c.) 15 minutes d.) 20 minutes and e.) 30 minutes from a case in the SP that took place from October 09, 2018 to October 23, 2018.

To determine which rain rate relationship will best represent the convective/stratiform fractions for each region, sensitivities among the different relationships were evaluated. Fig. 2.3 shows the sensitivities among 2 different rain-rate relationships. These relationships are calculated differently and use dual-polarization variables (Fig. 2.3a) and single-polarization variables (Fig. 2.3b). The sensitivities to these relationships are very similar and they paint a consistent picture in terms of the fractions of convective rainfall. With that being said, to use a longer temporal period for radar data (i.e., cases before 2013 when Dual Pol was unavailable), using the mid-latitude Z-R relationship and the tropical Z-R relationship, along with the hybrid stratiform relation to assess the fractions associated with convection and stratiform, is sufficient for the goal of this study.

To summarize, the steps that are taken in this study are as follows:

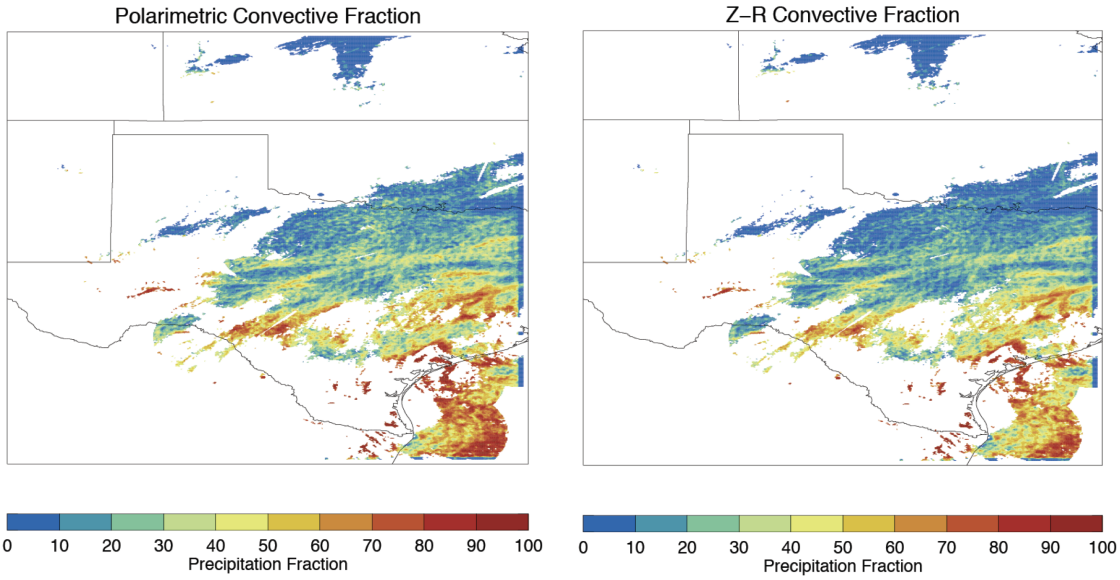

Figure 2.3: Total convective fraction for a.) polarimetric relationship and b.) mid-latitude Z-R relationship from a case in the SP that took place from October 09, 2018 to October 23, 2018.

1. Create 15-minute GridRad data for each of the 27 events.

2. Classify echoes at each GridRad time as either convective or stratiform using SL3D.

3. Estimate rain rates from the radar observations at each GridRad time and accumulate the rainfall from the convective/stratiform echoes separately for rainfall fraction analyses.

4. Leverage convective/stratiform rainfall fractions for event evaluation to characterize the dominant source of precipitation.

5. Analyze synoptic patterns to identify drivers of each event (see Section 3.2).

To determine the dominant source of precipitation, there are three metrics that are leveraged in this study. The first metric is to find how much of the extreme area is dominated by convection. Additionally, in these extreme areas dominated by convection, the average convective rain fraction was also found. Thirdly, by weighting

the total PRISM precipitation volume in each grid box by the radar-determined rain fraction, the amount of precipitation that was caused by each source is calculated. By using these metrics, the dominant source of precipitation and the amount of precipitation from that source for each case can be found and will be used for physical understanding. Effectively, the physical characteristics of each event give insight about the synoptic patterns and the forcings at play in creating that event, which say something about how well that event might be forecast on a climate scale. Using the aforementioned atmospheric variables in Section 2.1 for 250 hPa, 500 hPa, 850 hPa, and surface analyses, the primary driving mechanisms for each event can be evaluated. In addition, these synoptic-scale features will be able to help distinguish which Z-R relationship is more relevant for each case. In turn, this will give the most appropriate value of convective dominance, which will eventually give understanding about the microphysics for the case.

Chapter 3

Results

3.1 Synoptic Evaluation

Previous research on distinct synoptic patterns associated with extreme precipitation events has been well-documented throughout recent history. Short duration extreme precipitation events in North America have been characterized to have synoptic fronts, orographic ascent, and atmospheric rivers across many regions (Barlow et al., 2019). Although these characteristic patterns are not at the S2S scale, they may shed light on repeating patterns within the S2S time frame. Jennrich et al. (2020) found that for 14-day S2S events, 500-hPa geopotential heights and integrated vapor transport (IVT) were good variables to assess leading synoptic patterns for extreme precipitation across the CONUS. IVT is a measure of vertically integrated column of moisture from 1000 hPa to 200 hPa. Smith et al. (2010) studied 3 floods along the Delaware River basin and found that strong moist flow at 850 hPa was a key contributor to the flooding. Another study found that anomalous values of PWAT play a significant role in urban flooding across the CONUS (Schroeder et al., 2016). Using geopotential heights at 250 hPa and 500 hPa with wind speeds help show the large-scale forcings from the upper troposphere, and focusing on moisture variables at the 850 hPa level and the surface help show how deep the moisture is for each case. In addition, temperature advection at the 850 hPa level can help gain an understanding of rising motion above that layer owing to the quasi-geostrophic (QG) equation (Bluestein, 1992).

3.1.1 Example Case

This section is designed to highlight a single case and outline the step-by-step process that was used for each case for the synoptic evaluation. For the example case, SP20090426 will be used from Section 2.2.1. Fig. 3.1 shows the total daily precipitation from PRISM for SP20090426 with only the precipitation associated with the extreme grid points plotted. From this figure, it appears that 4/27-4/30, 5/2-5/3, 5/6, and 5/8 were the days that produced the majority of precipitation, therefore, these are the days that will be the primary focus of this analysis.

A top-down approach is used to assess the synoptic characteristics, starting with 250 hPa. Maps of 250hPa with 3-hour increments from MERRA-2 include geopotential heights (dam) and wind (in kts). From these maps, troughs/ridges and jet streaks/maxima can be analyzed. Fig. 3.2 shows an example of what a 250 hPa analysis map looks like. In this figure, a longwave trough was evident with the trough axis upstream of the region. In addition, a jet streak with roughly 60-70 $ms^{-}1$ flow was orientated southwest to northeast along the Rocky Mountains. Another strong jet maxima was located over Ontario/Quebec, Canada which acted to strengthen the shortwave ridge downstream of the SP.

Fig. 3.3 shows the same variables as Fig. 3.2, but for 500 hPa. In this figure, a longwave trough was also apparent across the MW with jet streaks located along the base and downstream of the trough, and another weaker jet streak upstream of the trough axis over the northwestern CONUS. These jet streaks allow the trough to dig further to the south and helped provide large-scale ascent over the region (discussed later in this Chapter). In addition, another strong jet streak was located along the border of Ontario and Quebec, Canada. In turn, the shortwave ridge downstream of the SP would build, and the longwave trough upstream of the SP remained in place, allowing for longer duration of large-scale ascent.

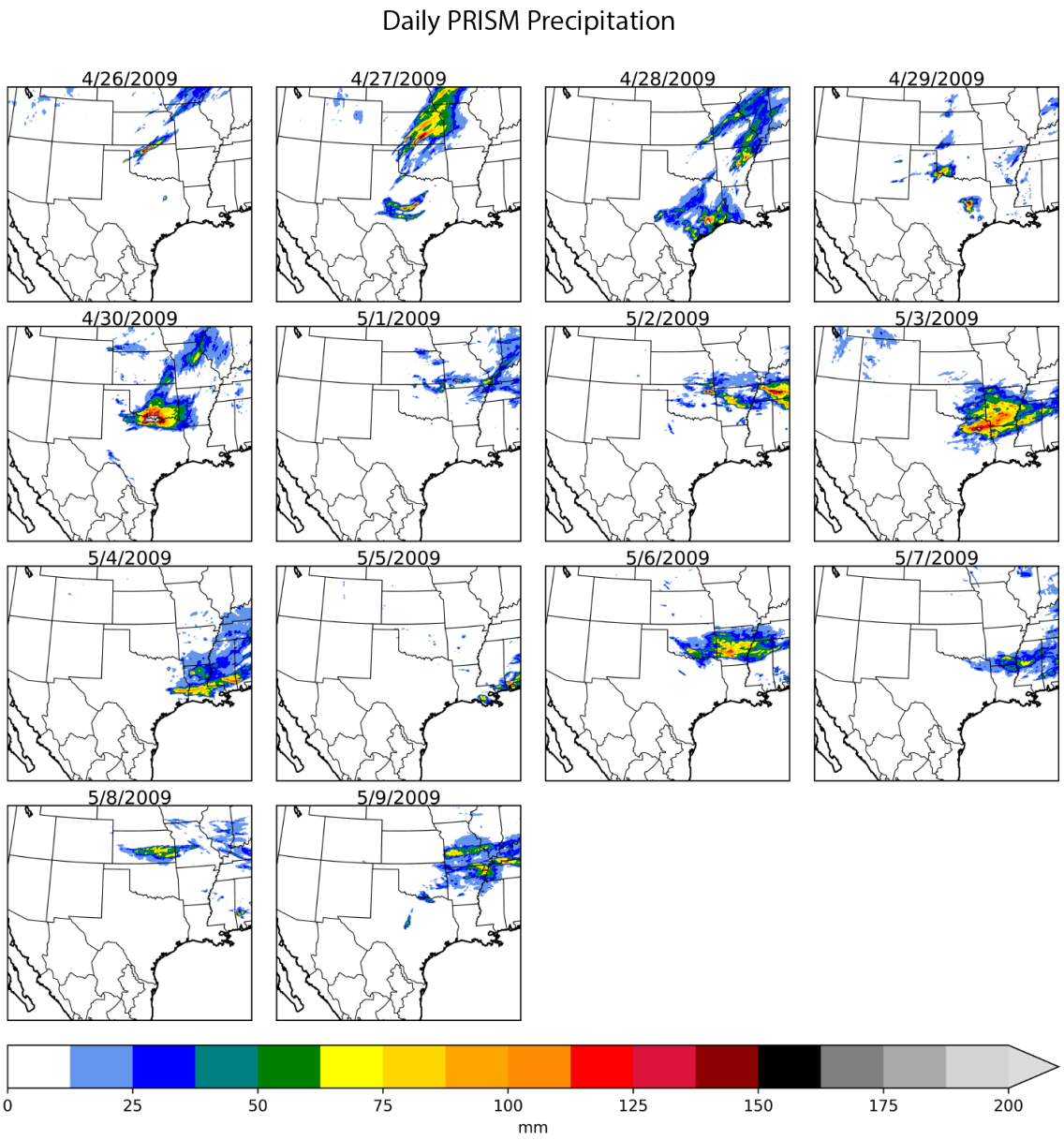

Figure 3.1: Total daily precipitation (mm) from PRISM for a case in the SP from April 26, 2009 to May 09, 2009. Only grid points labeled as extreme have precipitation plotted.

Fig. 3.4 shows an 850 hPa analysis map for SP20090426. Over the SP, there was strong southerly low-level jet (LLJ) that was transporting warm, moist air over the region. Two areas of 850 hPa higher pressure can be seen over the Atlantic coast and over the Ontario/Quebec, Canada border. This was due to the broad ridge over

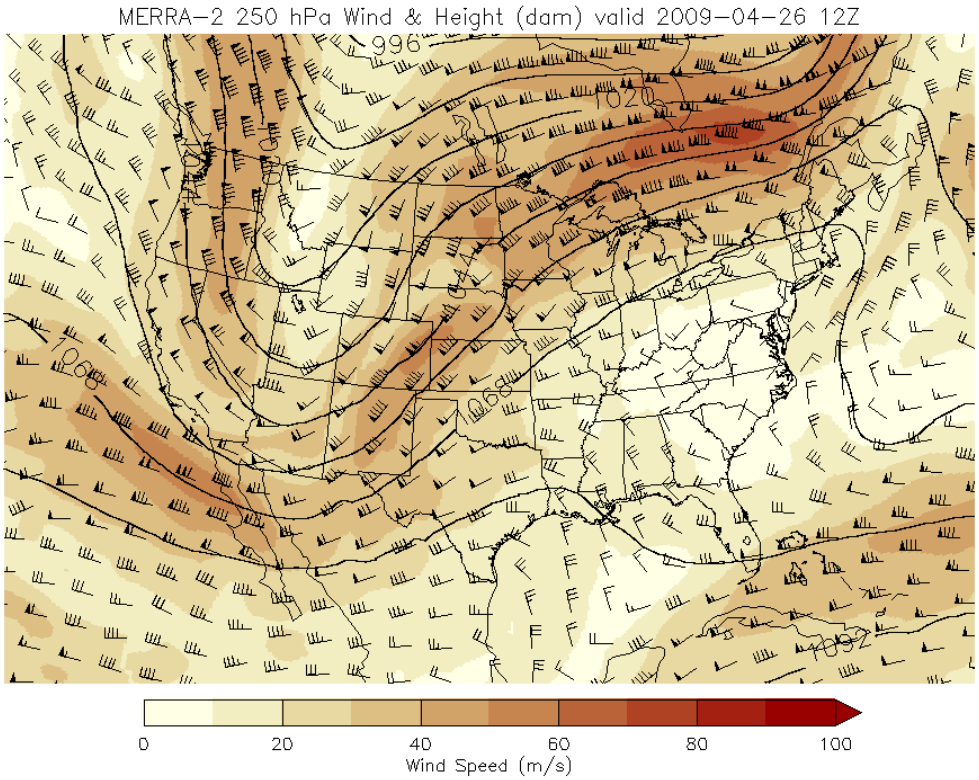

Figure 3.2: MERRA-2 250 hPa map with wind and geopotential height (dam) for SP20090426 at 12Z. Filled contours represent wind (m/s).

the Atlantic coast and shortwave ridge that was overspreading the NP/GL regions. A broad swath of high RH was also evident from the strong flow over the SP. With an upper level longwave trough pattern upstream and a broad ridge downstream of the region, the 850 hPa response was going to result in strong low-level southerly advection. The 850 hPa isotherms were perpendicular to the flow along and over west-central Texas, which resulted in warm air advection (WAA) later in the case. WAA at this level is important for large-scale ascent as it promotes rising air from isentropic ascent.

Fig. 3.5 shows two surface analyses, one from MERRA-2 and the other from WPC. In this figure, there is lee troughing along the Rockies associated with the mid-level trough that is allowing for southerly flow at the surface. It is evident that this

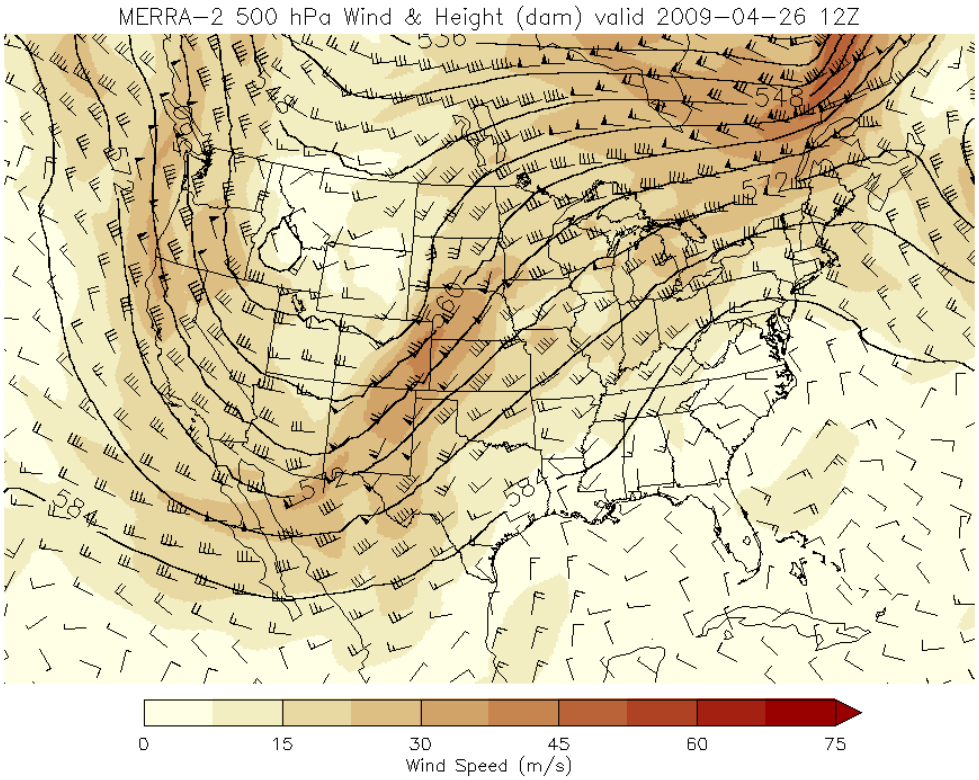

Figure 3.3: As in Fig. 3.2, but for 500 hPa.

surface flow is bringing in a moderately moist airmass from the Gulf of Mexico, and this moisture advection extends into the low-to-mid-levels (high PWAT values over the region). In addition, there is a synoptic warm front that was situated along the western Texas/Oklahoma panhandle, and extends into central Kansas and along the Iowa/Missouri border. These ingredients all collocated with one another combined to produce the rainfall for the first day in the 14-day event.

The information presented above for the one day in this case, is how every day of the 14-event is analyzed. Key features at 250 hPa include troughs/ridges and jet maxima; at 500 hPa include troughs/ridges and jet maxima; at 850 hPa include WAA/CAA and associated upper-level fronts, direction of flow, high RH, cyclones or anticyclones, and speed maxima; at the surface include synoptic fronts/boundaries,

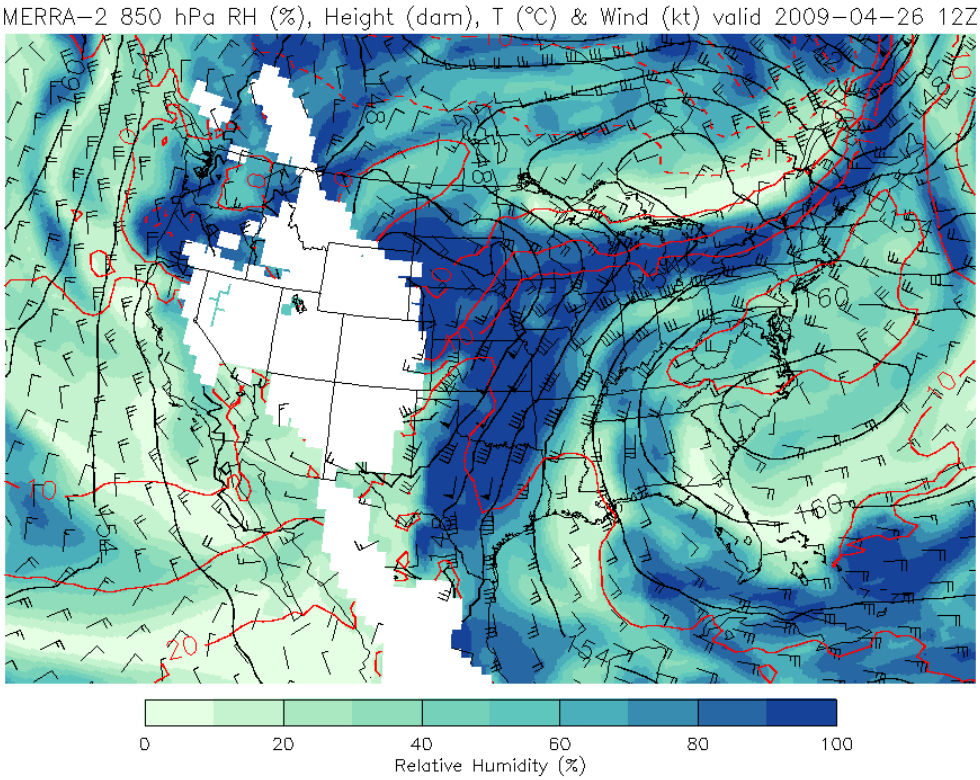

Figure 3.4: MERRA-2 850 hPa map with relative humidity (%), temperature (°C), wind (kt), and geopotential height (dam) for SP20090426 at 12Z. Filled contours represent relative humidity (%).

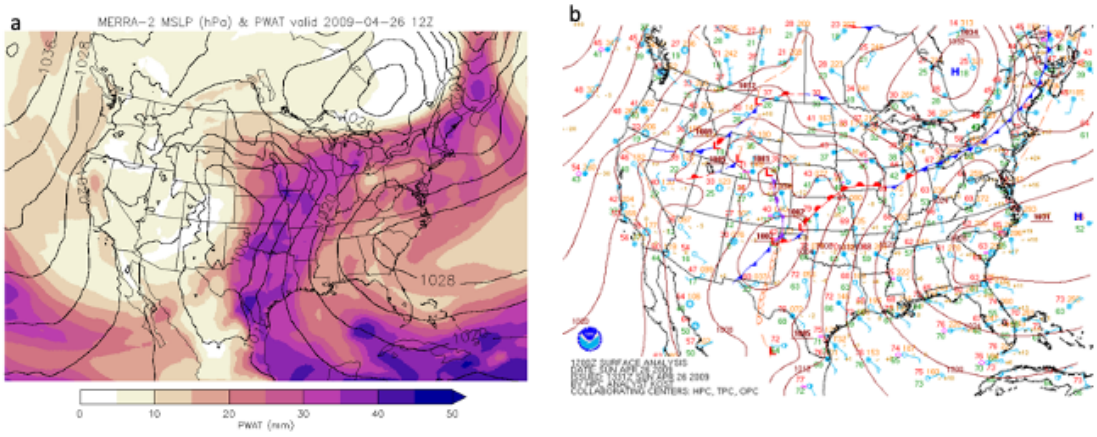

Figure 3.5: Surface map from a.) MERRA-2 with MSLP (hPa) and contoured PWAT (mm), and b.) WPC with MSLP, station plots, and frontal/synoptic boundaries for SP20090426 at 12Z.

cyclones/anticyclones, orientation of flow, and high PWAT. In addition to these features, event statistics were also identified to fully characterize which Z-R relationship bet suits each case. For example, SP20090426 will be classified as predominantly mid-latitude environment, rather than a tropical environment. If there are any discrepancies on whether a case is mid-latitude or tropical, looking at archived environmental soundings for each case can help solidify the choice between mid-latitude and tropical environments.

3.2 Regional Synoptic Characteristics

3.2.1 Southern Plains

In the SP, there were 6 events that were highlighted for the analysis of this study, all of which took place in the late spring/early summer months. Table 3.1 shows the synoptic characteristics of each event in the SP. Of these events, 3 were characterized as tropical environments, and 3 were characterized as mid-latitude environments. One of the key distinguishing factors between the tropical environments and mid-latitude environments in this region was at the 850 hPa level. Among the mid-latitude environments, there was either WAA or CAA at 850 hPa, whereas for the tropical environments, there was no temperature advection. Similarly, however, deep moisture advection seemed to be a characteristic that all of the cases shared and there was at least one boundary over the areas that experienced precipitation.

At 250 and 500 hPa, the commonality amongst all but 1 of the cases was a trough (either longwave or shortwave) that was positioned upstream of the region. These troughs were more pronounced and dug further south among the cases that had mid-latitude characteristics. This makes intuitive sense as these cases occurred in the middle of spring where the equator-to-pole temperature gradient is still large enough to support upper-level flow that far south. In addition, jet streaks were a contributing factor to not only the propagation of the trough itself, but the large-scale rising motion

Extreme Event Synoptic Characteristics for the SP						
Event	**Tropical or Mid-lat?**	**Trough?**	**Number of Troughs in Case**	**WAA or CAA at 850 hPa**	**High RH and PWAT?**	**Surface Fronts or Boundaries**
SP20090426	Mid-lat	Y	5	WAA	Y	Warm front and stationary front
SP20100514	Mid-lat	Y	3	WAA	Y	Warm front and stationary front
SP20100604	Tropical	Y	3	None	Y	Outflow boundary
SP20100627	Tropical	Y	1	None	Y	Outflow boundary
SP20120502	Mid-lat	Y	2	CAA	Y	Cold front
SP20130724	Tropical	N	0	None	Y	Outflow boundaries

Table 3.1: Table illustrating general characteristic patterns for all cases in the SP. The date indicated after SP represents the starting date for the 14-day event.

over the region. Jet streaks typically occurred upstream of the trough axis, which acts to help the trough dig deeper south. Another key upper level feature that distinguishes the mid-latitude environments from the tropical environments, is the position of the ridge. In the mid-latitude environments, a ridge is typically positioned downstream of the region; whereas, in the tropical environments, a ridge is directly overhead. This difference is very important for the large-scale forcings within each environment. From a QG framework, a trough axis upstream of the region will foster differential cyclonic vorticity advection (DCVA), thus promoting rising motion over the region (Bluestein, 1992). This trough-ridge pattern and associated ascent will promote the development of precipitation, and has been tied to heavy rainfall (Maddox et al., 1979).

At the 850 hPa level, areas of WAA or CAA are what delineates mid-latitude from tropical environments. In Table 3.1, all three mid-latitude cases experience some sort of temperature advection, whereas the tropical environments did not. At this level,

all cases experienced high RH on days that experienced precipitation. A southerly LLJ was common for these cases and was the primary transport of deep moisture that overspread the SP. For SP20090426 and SP20100514, a downstream 850 hPa anticyclone was in place for majority of the 14-day events. This downstream anticyclone, coupled with cyclogenesis from lee troughing, helped aid in stronger warm, moist air advection over the region. Isentropic ascent coupled with moisture advection at the 850 hPa level allows for the environments to be primed for precipitation. On the other hand, for SP20120502 where CAA took place, the CAA itself was not responsible for the rising motion, but the cold front aloft (CFA) itself was responsible for the rising motion.

At the surface, there were synoptic boundaries for all 3 of the mid-latitude cases and weak outflow boundaries or no boundaries for the tropical cases. All cases experienced high PWAT values on days that experienced precipitation. For SP20090426 and SP20100514, a synoptic warm front was evident and help to provide lift at the surface. A strong cold front was the primary driver for SP20120502, where the frontal boundary tilted with height up to 850 hPa. The aforementioned outflow boundaries for the tropical cases are not synoptically driven, but are still important for rising motion during the summer months. During the summer months in the SP, high surface temperatures coupled with high moisture content only need weak upward motion in order to reach the lifted condensation level (LCL). Any lingering outflow boundaries or sea-breeze boundaries can act as a mechanism to enable a parcel to reach its LCL. Besides SP20100627, where a majority of the precipitation fell from the outer bands of Hurricane Alex, precipitation from the other two tropical cases was initiated by these outflow boundaries. With weak steering flow aloft (i.e., weak 500 hPa winds), the precipitation that fell was likely caused by multicellular storms that remained over a single region.

Extreme Event Statistics for the SP						
Event	Tropical Convective Dominance	Mid-lat Convective Dominance	Average Tropical Convective Rain Fraction	Average Mid-lat Convective Rain Fraction	Tropical Convective Precipitation Magnitude	Mid-lat Convective Precipitation Magnitude
SP20090426	83.76	**59.47**	73.71	**67.54**	68.69	**55.35**
SP20100514	86.09	**68.12**	77.39	**71.14**	67.09	**55.9**
SP20100604	**93.84**	81.47	**80.61**	72.97	**76.32**	64.81
SP20100627	**81.53**	52.21	**70.81**	64.56	**57.19**	44.78
SP20120502	59.5	**34.27**	69.85	**66.61**	47.24	**36.35**
SP20130724	**78.39**	55.17	**75.89**	72.19	**62.49**	49.15

Table 3.2: Table illustrating the event statistics for the SP. The first column is the event name with the starting date of the event. The second and third column are the percentages of the extreme area dominated by convection for the tropical and mid-latitude relationships, respectively. The fourth and fifth column are the average convective rain fraction in areas dominated by convection for the tropical and mid-latitude relationships, respectively. The sixth and seventh columns represent the total PRISM precipitation volume fraction from convection within the extreme event area and given by the tropical and mid-latitude relationships, respectively. All values are represented as percentages. Bold numbers correspond to values determined by the event characteristics.

Table 3.2 shows the statistics for each of the cases in the SP. For SP20090426, SP20100514, and SP20120502 using the mid-latitude Z-R relationship is more appropriate given the synoptic characteristics, and for SP20100604, SP20100627, and SP20130724 using the tropical Z-R relationship is more appropriate. In this region, convection is the dominant source of precipitation, and the precipitation that fell in the extreme grid points was predominately convective rain. The only case not dominated by convection was SP20120502, where stratiform was the dominating source.

3.2.2 Southeast

In the SE, there were 6 events that were highlighted for the analysis of this study and ranged from early spring through winter. Table 3.3 summarizes the synoptic characteristics of each event in the region. Of the 6 events, 4 were characterized as mid-latitude environments, and 2 were characterized as tropical environments. There were 3 key features that distinguished between these environments. The first difference is that there were no upper-level troughs associated with tropical environments,

whereas troughs were evident in each of the mid-latitude cases. In addition, there was no advection of temperature or frontal boundaries at the 850 hPa level in the tropical environments. Lastly, the surface boundaries for the mid-latitude cases were more synoptic-scale fronts, whereas in the tropical cases, more mesoscale boundaries (i.e., outflow boundaries) were evident. All cases, however, experienced high RH at 850 hPa and high PWAT on days that experienced precipitation.

At 250 hPa and 500 hPa, there were two distinct patterns among the mid-latitude cases. The first pattern among these cases included a longwave trough upstream of the region and a blocking longwave ridge downstream of the region. A jet streak over the SE between the trough axis and ridge axis eventually would move through the ridge and help maintain a blocking pattern. In turn, this allowed for consistent DCVA overspreading the SE. The other pattern associated with the mid-latitude cases was a constant trough/shortwave trough training pattern over the entire region. This includes a longwave trough pattern with embedded shortwaves moving through the region. In both patterns, large-scale rising motion was in place for the onset of precipitation. For the tropical cases, however, no troughing was evident in any of the days that produced precipitation. In fact, ridging along the NP with weak flow over the region was the primary pattern during precipitating days. This type of flow pattern is expected given that these 2 cases took place in late summer/early fall where the subtropical jet (STJ) is positioned along the northern CONUS.

At 850 hPa, areas of WAA and CAA took place in the mid-latitude cases, and no advection of temperature took place in the tropical cases. All 6 cases had high relative humidity at this level, regardless of the the temperature advection that took place. For the tropical cases with weak 850 hPa flow, consistent southerly flow from the Gulf of Mexico helped to provide deep moisture for parcels that could reach the LCL. For the mid-latitude cases, an 850 hPa cyclone was present upstream of the region. This provides strong warm, southerly flow and moisture advection into the

Extreme Event Synoptic Characteristics for the SE						
Event	**Tropical or Mid-lat?**	**Trough?**	**Number of Troughs in Case**	**WAA or CAA at 850 hPa?**	**High RH and PWAT?**	**Surface Front or Boundaries?**
SE20090326	Mid-lat	Y	2	WAA and CAA	Y	Cold and Warm Fronts
SE20090430	Mid-lat	Y	3	WAA	Y	Warm Front and Stationary Boundary
SE20090910	Tropical	N	0	None	Y	Outflow Boundaries
SE20120709	Tropical	N	0	None	Y	Outflow Boundary
SE20151217	Mid-lat	Y	5	WAA and CAA	Y	Cold and Warm Fronts
SE20170422	Mid-lat	Y	3	CAA	Y	Cold and Warm Front

Table 3.3: As in Table 3.1, but for the SE.

region. In addition, for SE20090326, SE20151217, and SE20170422, there was CAA and associated cold front ahead of the open warm sector that swept through the region. These deep baroclinic zones that extended aloft were the primary forcings for the precipitation that fell in these cases.

At the surface, a cyclone and attendant synoptic boundaries were all present in each of the mid-latitude cases, and mesoscale boundaries were present in the tropical cases. For SE20090326 and SE20151217, a strong surface cyclone in the GL/NP vicinity was not only responsible for the WAA over the SE, but also the strong cold front that swept through the region and provided surface-based lift for the onset of the precipitating days. The strong surface boundary, coupled with the upper-level large-scale forcing from the upstream longwave trough, was the primary reason for the extreme precipitation in the SE for these cases. For SE20170422, a weak surface cyclone developed over central Texas and moved through the region. An associated warm front that accompanied this cyclone provided the surface-based ascent necessary to enable parcels to reach their LCLs. For the tropical cases, the primary surface-based mechanisms for ascent were outflow or sea-breeze boundaries. With

Extreme Event Statistics for the SE						
Event	Tropical Convective Dominance	Mid-lat Convective Dominance	Average Tropical Convective Rain Fraction	Average Mid-lat Convective Rain Fraction	Tropical Convective Precipitation Magnitude	Mid-lat Convective Precipitation Magnitude
SE20090326	37.56	**16.89**	65.85	**60.64**	45.5	**32.36**
SE20090430	60.96	**24.04**	64.88	**60.78**	55.63	**40.49**
SE20090910	**76.97**	53.25	**73.62**	67.92	**64.92**	51.66
SE20120709	**89.42**	78.52	**81.17**	74.29	**75.89**	64.48
SE20151217	36.18	**13.41**	66.44	**60.78**	41.18	**28.52**
SE20170422	43.04	**24.51**	70.94	**67.62**	48.17	**35.84**

Table 3.4: As in Table 3.2, but for the SE.

weak upper-level flow, negligible large-scale ascent, and high PWAT, multicellular storms were most likely the dominating storm-type for the two tropical cases.

The event statistics for each of the cases in the SE are provided in Table 3.4. For the mid-latitude cases, the dominating precipitating source was stratiform precipitation. In addition, in these areas dominated by stratiform, the precipitation volume is also dominated by stratiform precipitation. The tropical cases, however, are strongly dominated by convection. Given the time of year of all of these events, the dominating source in all of the cases sheds light on what precipitation can be expected for a given time of year in the SE.

3.2.3 Northern Plains

In the NP, there were 5 events that were highlighted for the analysis of this study, all of which took place in late spring/summer time frame. All 5 of these events were characterized as mid-latitude environments (Table 3.5). All of the events had an upper-level trough over the region and some advection of temperature at 850 hPa. All surface boundaries associated with precipitation for these events were on the synoptic scale. In addition, high RH and high PWAT values were evident on the days that experienced precipitation.

At the 250 hPa and 500 hPa level, there was a mixture of different patterns that aided the onset of precipitation. Firstly and more commonly, a longwave or shortwave trough was typically located just upstream of the region of precipitation. In turn, this provided the DCVA necessary for large-scale rising motion over the area. The next pattern that was associated with precipitation was a zonal flow pattern with embedded jet streaks. As the jet streak moved over the region, the areas that were favorable for synoptic scale lift were the front right and back left regions of the jet. These regions are where upper-level divergence occurs owing to the ageostrophic response to the jet maxima in the entrance/exit regions of the jet (Bluestein, 1993). The third pattern is ridging over the region with northwest flow aloft. This type of pattern will foster lee cyclogenesis along the Rocky Mountains, which can support moisture advection at 850 hPa into the region. A pattern that was not as common, but still impactful was a ridge upstream of the region near the Rocky Mountains. This type of pattern supports higher pressure at the surface between the ridge axis and downstream trough axis. Areas that are south of the surface anticyclone will experience easterly flow that transports moist air up the mountain range. In turn, this air condenses and turns into a cluster of storms. The northwest flow aloft acts as steering flow and transports, what turns into a mesoscale convective system (MCS), over the region.

Every single case was aided by the deepening of an 850 hPa cyclone that moved through the region. These cyclones were typically accompanied by strong southerly flow ahead of a CFA and would remain over the region as a downstream anticyclone stayed in place over the Atlantic coast. Not only does the strong southerly flow provide moisture advection in the region, but it also promotes large ascent and support for excessive precipitation. In fact, each regional event had at least one day of precipitation where a LLJ was present on that day. Given the time of year of the cases, consistent flow over the Rocky Mountains supports cyclone formation just east of the

Extreme Event Synoptic Characteristics for the NP						
Event	**Tropical or Mid-lat?**	**Trough?**	**Number of Troughs in Case**	**WAA or CAA at 850 hPa?**	**High RH and PWAT?**	**Surface Front or Boundaries?**
NP20110614	Mid-lat	Y	3	WAA and CAA	Y	Cold and Warm Fronts
NP20130519	Mid-lat	Y	2	WAA	Y	Stationary Boundaries
NP20140602	Mid-lat	Y	3	WAA and CAA	Y	Cold and Warm Fronts
NP20160420	Mid-lat	Y	3	WAA and CAA	Y	Cold and Warm Fronts
NP20170813	Mid-lat	Y	4	WAA	Y	Cold/Warm Front and Stationary Boundaries

Table 3.5: As in Table 3.1, but for the NP.

mountain range over the NP. High RH overspread the region, especially around the 850 hPa cyclone.

The positioning of the surface cyclone and associated synoptic boundaries varied among the precipitating days in each event. In each of the events, there were two different distinct surface patterns. The first pattern was a surface cyclone that developed in central Kansas. As the cyclone moved towards the northeast, CAA wrapped around the surface cyclone over the extreme areas that experienced precipitation. The second pattern was a surface cyclone that developed along the lee of the Rocky Mountains in North Dakota and sometimes further south into the South Dakota/Nebraska border. With this type of pattern, a warm front and attendant WAA overspread the region, while a cold front swept through as the surface continued to moved towards the GL region. With both of these scenarios, high PWAT (relative to the NP) was in place over the region for the onset of precipitation. In addition, some events experienced convergence along surface troughing and stationary boundaries leftover from surface cyclones. The primary forcing mechanisms for ascent at the surface, however, were the warm fronts and the cold fronts that each of the events experienced in at least one of the precipitating days.

Extreme Event Statistics for the NP						
Event	Tropical Convective Dominance	Mid-lat Convective Dominance	Average Tropical Convective Rain Fraction	Average Mid-lat Convective Rain Fraction	Tropical Convective Precipitation Magnitude	Mid-lat Convective Precipitation Magnitude
NP20110614	35.06	**19.31**	68.76	**65.92**	26.98	**19.75**
NP20130519	42.24	**27.34**	71.2	**65.55**	36.43	**27.4**
NP20140602	57.63	**35.58**	70.31	**65.43**	49.6	**37.7**
NP20160420	8.94	**3.81**	65.6	**65.53**	16.19	**10.4**
NP20170813	75.02	**54.88**	74.01	**67.31**	62.71	**50.43**

Table 3.6: As in Table 3.2, but for the NP.

Table 3.6 shows the event statistics for the all of the cases in the NP. In all but one case (NP20170813), the dominating precipitating source was stratiform, where percentages of convective dominance varied from 3.81% to 35.58% (column 3 of Table 3.6). In these areas dominated by stratiform, the precipitating volume is also dominated by stratiform precipitation. From a physical viewpoint, large-scale rising motion from upper-level DCVA, 850 hPa WAA, and the synoptic surface boundaries are responsible for the dominance in stratiform precipitation in the extreme areas. For NP20170813, however, convection was not only the dominating precipitating source, but the precipitating volume was convectively dominant as well. One hypothesis to this difference is the fact that this case had a stationary boundary that remained over the region, whereas the other cases had frontal boundaries that would move through the region. The reasoning behind this hypothesis is that in the summertime surface temperatures are warm beneath steep mid-level lapse rates, so convergence along this boundary fosters continuous forced ascent over a large area and thus, favorable for precipitation.

3.2.4 Great Lakes

In the GL, there were 5 events that were highlighted for the analysis of this study, which ranged from late spring to late summer (Table 3.7). In this region, all 5 events were characterized as having mid-latitude environments for the onset of the

precipitation. There were a lot of synoptic-scale features that were similar amongst these cases. For example, at least 3 days in each event that produced precipitation had a trough move through the region. In addition, every event experienced days with WAA or CAA at 850 hPa during precipitating days. In some cases, however, a CFA swept through the region behind areas of WAA. Both warm fronts and cold fronts were in place in these events to foster rising motion at the surface. Finally, every event had high RH at 850 hPa and high PWAT on days of precipitation.

At 250 hPa and 500 hPa, very similar patterns occurred on days that produced precipitation. A trough was usually situated with the trough axis over the Rocky Mountains along the Colorado/Kansas border and southwest flow over the region. A broad, downstream ridge would build over the northeast CONUS, allowing for continuous DCVA over the entire region. In addition, jet streaks within the upper flow would add additional dynamical lift as they propagated through the region. For example, the strongest jet streak that occurred in any event was in GL20160904, specifically on September 7, 2016 at 00Z. The jet streak, which reached upwards of 120 kts, was elongated and oriented from southwestern Nebraska to northern Minnesota. The large scale rising motion from the jet streak dynamics played a big role in the widespread precipitation over the whole region. In fact, this same jet streak moved through the ridge and helped to build the ridge and keep the upstream trough in place. This trough-ridge pattern was very common amongst the cases.

At 850 hPa, the common pattern amongst all the cases was a deepening cyclone in the NP or even southern Canada. This deepening cyclone would allow for warm, moist air to be advected northward into the region. If the downstream ridge began to build, then the 850 hPa cyclone would stay in place over the region with a CFA moving over the region and high RH ahead of the front. In addition, high RH seemed to also wrap around to the north side of the cyclone, as a secondary location for precipitation development (i.e., an occlusion and trough of warm air aloft). The cold

Extreme Event Synoptic Characteristics for the GL						
Event	**Tropical or Mid-lat?**	**Trough?**	**Number of Troughs in Case**	**WAA or CAA at 850 hPa?**	**High RH and PWAT?**	**Surface Front or Boundaries?**
GL20110614	Mid-lat	Y	4	WAA and CAA	Y	Warm Front
GL20130520	Mid-lat	Y	4	WAA and CAA	Y	Cold, Warm, and Stationary Fronts
GL20140617	Mid-lat	Y	3	WAA and CAA	Y	Cold and Stationary Fronts
GL20160904	Mid-lat	Y	3	WAA and CAA	Y	Cold Fronts
GL20170612	Mid-lat	Y	3	WAA and CAA	Y	Cold Fronts

Table 3.7: As in Table 3.1, but for the GL.

front on the back side of the cyclone began to strengthen as the pressure gradient tightened from a building anticyclone downstream. This tightening pressure gradient also aided in stronger advection of temperature, both CAA and WAA, over the region.

At the surface, there were 3 distinct patterns that were associated with precipitation, all involving the location and movement of the surface cyclone. The first pattern is for the surface cyclone to develop to the west of the region, along the lee of the Rocky Mountains. With this pattern, the surface cyclone would bring warm, moist air northward. This is especially true for Minnesota and Wisconsin, where moisture from evapotranspiration in Iowa is advected northward. The surface cyclone would then move towards the northeast and a cold front associated with the cyclone would sweep through the area. The second pattern is the development of a cyclone along the northern periphery of the SP. When this cyclone moves towards the northeast into the region, the extreme area is north of the cyclone where CAA wraps around the cyclone to the east. The third pattern is a cyclone developing in Canada north of North Dakota. This pattern is the most common amongst all of the events. As the cyclone develops and deepens, warm air is drawn northward over the region. When the cyclone moves towards the east, a cold front sweeps through the entire region,

Extreme Event Statistics for the GL						
Event	Tropical Convective Dominance	Mid-lat Convective Dominance	Average Tropical Convective Rain Fraction	Average Mid-lat Convective Rain Fraction	Tropical Convective Precipitation Magnitude	Mid-lat Convective Precipitation Magnitude
GL20110614	80.76	**59.88**	74.63	**67.19**	66.74	**53.8**
GL20130520	67.86	**30.84**	65.78	**59.61**	57.09	**42**
GL20140617	91.92	**70.64**	74.67	**65.88**	72.36	**58.37**
GL20160904	69.68	**34.58**	67.15	**61.31**	57.75	**42.78**
GL20170612	73.38	**49.44**	72.09	**65.21**	61.35	**47.91**

Table 3.8: As in Table 3.2, but for the GL.

allowing for large-scale ascent. In all of these different patterns, high PWAT is in place before the fronts move through for the onset of precipitation.

Table 3.8 shows the statistics for all 5 of the events in the GL. Of the 5 cases, 2 of them had convection as the dominating source, and 2 had stratiform as the dominating source. GL20170612 was almost exactly 50/50 for convective/stratiform dominance, here will say that this case was marginally convective dominant. For GL20110614 and GL20140617, the average convective rain fraction in areas that were convectively dominated was at least 65%. In these areas of convective dominance for GL20110614 and GL20140617, the convective precipitation magnitude was 53.8% and 58.37%, respectively. For these two cases, not only was convection the dominating source of precipitation, but the precipitation that fell in the extreme areas were predominately convective precipitation. For GL20130520, GL20160904, and GL20170612, stratiform was the dominating source of precipitation. For the precipitation magnitude in these events, precipitation that fell from the stratiform echoes produced the majority of the precipitation for the event. Based off these statistics, stratiform precipitation is the dominating source, especially in the late spring to early fall time frame.

3.2.5 Northeast

In the NE, there were 5 events that were used in the analysis of this study, all of which were characterized as having mid-latitude environments. These 5 events

spanned from late winter to late fall (Table 3.9). There were similarities and differences in the synoptic features amongst the cases. For example, each of the events had a least 2 upper-level troughs that were supportive of precipitation. In addition, CAA and WAA were evident over the region at 850 hPa. The magnitude of the temperature advection at 850 hPa, however, differed depending on the time of year of the event. At the surface, every event in the region had a synoptic-scale boundary associated with precipitation. In some cases, a warm or cold front helped to produce precipitation and in other cases, a stationary or an occluded front lingered over the region.

At 250 and 500 hPa, the most common feature among the events was a longwave trough upstream of the extreme areas. In addition to this trough, a jet streak would form over the entire NE. The magnitude of this jet would change depending on the time of year (i.e., stronger surface temperature gradient in the fall/winter than in the summer), but the jet streak dynamics did not change. The jet streak dynamics coupled with the large-scale rising motion from DCVA downstream of the trough axis supports widespread precipitation throughout the region. Interestingly enough, the primary areas of precipitation on days with this particular upper-level pattern were focused on the right entrance and left exit regions of the jet. Another pattern that was more common in the late spring to early summer events was embedded shortwaves within a broader longwave trough. Perturbations within the broader longwave trough allow for localized enhanced areas of DCVA.

At 850 hPa, the common pattern amongst the cases was the positioning of a cyclone and associated temperature advection with the cyclone. One case in particular had a strong response to the upper-level flow pattern. NE20110226 had a longwave trough aloft and a strong jet streak upstream of the trough axis over the region. The 850 hPa response to this pattern was a deepening cyclone over the region with WAA upstream. The CAA, however, was positioned more equatorward than was is

Extreme Event Synoptic Characteristics for the NE						
Event	**Tropical or Mid-lat?**	**Trough?**	**Number of Troughs in Case**	**WAA or CAA at 850 hPa?**	**High RH and PWAT?**	**Surface Front or Boundaries?**
NE20110226	Mid-lat	Y	4	WAA and CAA	Y	Cold, Warm, and Stationary Fronts
NE20130607	Mid-lat	Y	4	WAA and CAA	Y	Cold, Warm, and Stationary Fronts
NE20150609	Mid-lat	Y	3	WAA and CAA	Y	Cold, Warm, and Stationary Fronts
NE20171025	Mid-lat	Y	2	WAA and CAA	Y	Cold and Occluded Front
NE20180513	Mid-lat	Y	3	WAA and CAA	Y	Cold Front and Stationary Front

Table 3.9: As in Table 3.1, but for the NE.

typically associated with a deepening 850 hPa cyclone. The reasoning behind this is because there was a trough of warm air aloft (trowal) that was wrapped around the cyclone. Fig. 3.6 depicts the trowal directly over the NE. The airstream associated with the trowal takes a cyclonic turn westward around the cyclone, and the warm conveyer belt turns anticyclonically eastward along the warm front (Han et al., 2007). In turn, the warm air cyclonically wrapping around the cyclone rises (and condenses) until it eventually sinks within the cold, dry air beneath.

Other patterns at 850 hPa were less complex, but just as effective at producing precipitation. For example, NE20130607 and NE20150609 events both had a cyclone develop upstream of the region, drawing in warmer air from the south and colder air from the north. In a QG framework, the upper-level response to this pattern is a deepening trough upstream and a building ridge downstream, thus strengthening the ageostrophic divergence aloft in the inflection point between the trough axis and the ridge axis. In turn, this tightened the height gradient and helped for stronger temperature advection over the region. In both of these events, the cyclone deepened

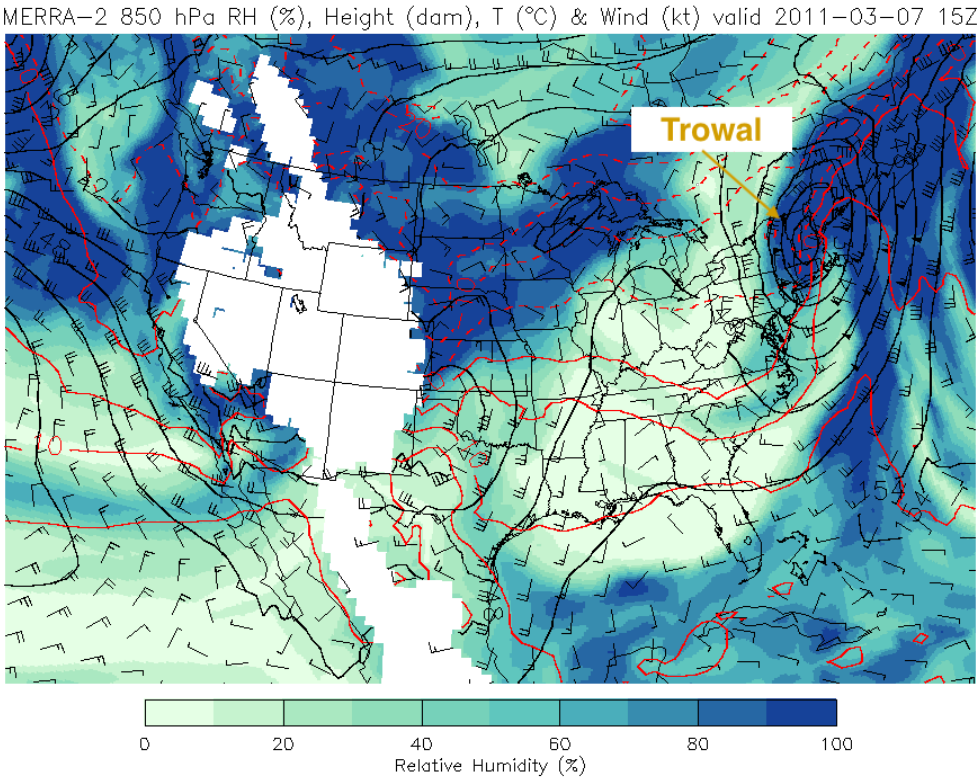

Figure 3.6: As in Fig. 3.4, but for 03/07/2011 at 15Z. Trowal is evident over the NE with high RH wrapping around the north and west side of the cyclone.

as it moved towards the northeast and a CFA moved through the extreme areas. All of the events in this region had regions of high RH on days where precipitation occurred.

At the surface, there were two distinct patterns among the 5 events. For NE20110226 and NE20171025, a cyclone at the surface continued to deepen as it moved through the region. The deepening cyclones would tend to follow the Atlantic coast line as the warm front associated with the cyclone remained parallel to the coast. The land-ocean temperature gradient, given the time of year for both of these events, explains why the warm front would tend linger around the coastline. The cold front associated with the deepening cyclone was strong and provided sufficient surface-based lift for precipitation. The other 3 cases, however had surface cyclones that were weak and

Extreme Event Statistics for the NE						
Event	Tropical Convective Dominance	Mid-lat Convective Dominance	Average Tropical Convective Rain Fraction	Average Mid-lat Convective Rain Fraction	Tropical Convective Precipitation Magnitude	Mid-lat Convective Precipitation Magnitude
NE20110226	0.08	**0.03**	68.81	**79.14**	2.89	**1.53**
NE20130607	30.33	**13.18**	65.53	**60.93**	34.43	**23.86**
NE20150609	61.76	**37.69**	69.88	**63.2**	53.19	**40.29**
NE20171025	0.23	**0.03**	59.22	**65.86**	7.6	**4.2**
NE20180513	67.11	**34.46**	67.63	**62.47**	57.52	**43.07**

Table 3.10: As in Table 3.2, but for the NE.

disorganized. The surface boundaries tended to stall and linger over the region, providing constant areas of horizontal vorticity that could be tilted and stretched into the vertical. For all events except NE20110226 and NE20171025, there were high PWAT in areas that received precipitation. For NE20110226, PWAT values of 20 mm were evident during the precipitating days and for NE20171025, PWAT did not reach above 40 mm, primarily because these events took place in the cool season.

The event statistics for the NE can be seen in Table 3.10. The dominating source of precipitation in all 5 of the cases is stratiform. The cases with the highest percentages of convective dominance were the cases that occurred in the late spring to early summer, and the cases with the lowest percentages of convective dominance occurred in the fall/late winter. The convective precipitation magnitude in areas of convective dominance was well below 50% in most cases, except for NE20150609 and NE20180513 where convective precipitation magnitude was 40.29% and 43.07%, respectively.

Chapter 4

Summary and Discussion

S2S extreme precipitation can generate multiple impacts throughout the economy and in society at large. While the primary focus of previous research has been on daily or sub-daily precipitation events, examining precipitation events on the S2S timescale was explored here. Using a database of 14-day extreme precipitation events and analyzing the dominant precipitating source of each event is an appropriate place to start in order to shed light on the characteristics of each event. Working in predefined geopolitical boundaries within the CONUS allow for more accurate representation of the synoptic drivers for each region.

In the SP, half of the events were characterized as tropical, and half were characterized as mid-latitude environments; all of which took place from late spring to summer. From Table 3.1, it appears that there is some seasonality with the characteristics of the events. From the events in this study, mid-latitude environments seem to take place in the late spring, while tropical environments are confined to the summer months. Intuitively, these findings are consistent with the positioning of the STJ over the U.S. In the beginning of summer, the STJ starts to position itself more poleward, as the equator-pole temperature gradient decreases. All of the events, except for one that occurred in the late summer, had a upper-level trough positioned upstream of the region that experienced precipitation. This type of dynamical forcing is similar to other studies that looked at the hydrometeorological environments of extreme rainstorms in the SP (Bradley and Smith, 1994; Smith and Younkin, 1972). Bradley and Smith (1994) characterized strong dynamical forcing events as having a strong shortwave, longwave trough, or cutoff low upstream up of the region. The jet stream configuration for the onset of precipitation in the SP events is similar to that

in Smith and Younkin (1972) (Figure 1 in Smith and Younkin (1972)). In fact, the positioning of the inflection point between the trough axis and ridge axis for these events are also similar in Smith and Younkin (1972), with the heaviest precipitation amounts in advance of the inflection point. The aforementioned upper-level pattern associated with precipitation will foster predominately southerly flow at 850 hPa. In turn, this will allow for warm, moist air to be advected into the region. Deep moisture and the transport of that moisture are common in extreme precipitation events (Bradley and Smith, 1994; Smith et al., 2010). In fact, Schroeder et al. (2016) found that urban flash flooding events across the CONUS were associated with anomalous values of PWAT that often exceeded the 99^{th} percentile. Mid-latitude environments in the SP are typically associated with cold fronts, warm fronts, or stationary fronts where as tropical environments are triggered from mesoscale boundaries (i.e., outflow boundaries). Convection was the primary source of precipitation in 5 of the 6 cases (Table 3.2). There is a high likelihood of convective dominant precipitation during the late spring to early summer in the SP because during this time of year surface temperatures are warm, deep moisture is advected into the region, and mid-level lapse rates are steep. With that being said, weak forcing should be sufficient to trigger the onset of precipitation.

In the SE, 4 of the 6 events were classified as mid-latitude and the other 2 were classified as tropical. It appears that in the winter and early-to-late spring, mid-latitude driven events are more likely than tropical events, similar to that of the SP. Keim (1996) investigated the synoptic and seasonal patterns of heavy rainfall events across the SE and found that frontal systems (especially cold fronts) were the primary mechanism for precipitation. In addition, this study found that tropical disturbances are more likely to occur in the summertime because of the lack of mid-tropospheric airflow and and the positioning of the Bermuda High. In the mid-latitude environments where precipitation occurred, there was either WAA or CAA

present, whereas in the tropical environments there was no temperature advection. Maddox et al. (1979) found similar results in mid-latitude cases with southerly WAA over regions of precipitation (Fig. 6b in Maddox et al. (1979)). For the mid-latitude cases, stratiform precipitation was the dominating source with percentages upwards of 86% (SP20151217). Tropical events, however were dominated by convection, with percentages upwards of 89% (Table 3.4). Here, the likelihood and intensity of convective precipitation increases in the summer owing to deep moisture in the lower troposphere, instability, and mesoscale boundaries that are focal points for convergence and subsequent upward motion.

In the NP, all 5 of the cases were characterized as mid-latitude environments. Of the 5 cases, 4 of them were dominated by stratiform precipitation (Table 3.6). The only case that was dominated by convection was a late summer case; the precipitation volume, however, was almost split 50/50 amongst convection and stratiform for this case. The most common upper-level pattern associated with precipitation was a trough positioned just upstream of the region. Flanagan et al. (2018) found that during pluvial years in the NP, positive height anomalies over the central western coast of the CONUS facilitate more storm systems to move through the region. In all 5 cases, a deepening cyclone was accompanied by strong southerly flow (LLJ), advecting moisture into the region. The positioning of the 850 hPa cyclone upstream of the region and associated WAA over the region, in tandem with DCVA from the upper-level trough, provided large-scale rising motion necessary for widespread precipitation in each of the events. At the surface, two distinct patterns fostered additional lift for precipitating systems. The first pattern consisted of cyclone development in central Kansas and the movement of the cyclone just downstream of the region. In turn, CAA wrapped around the cyclone and provided sufficient lift for precipitation. The second pattern consisted of cyclone development along the lee of the Rockies in North Dakota and further south into the South Dakota/Nebraska border. As this cyclone

moved towards the northeast, a cold front would traverse the region moving into the warm sector. From these patterns, it is evident that large-scale features such as an upper-level trough and surface cold front play a huge role in facilitating upward motion over a large domain. From a regional perspective, stratiform dominance fits the intuitive model primarily because deep moisture advection this far poleward is not as prominent as in the SP or SE, so instability is less than these regions. In addition, with limited moisture transport, LCLs are much higher than regions that are more equatorward, so a deeper synoptic boundary (i.e., cold front) is going to be necessary for parcels to reach their LCLs.

In the GL, all 5 of the events were characterized as mid-latitude environments. GL20110614 and GL20140617 were dominated by convective precipitation and precipitation magnitude, whereas the other 3 cases were predominately stratiform dominant. It appears that summertime is when there is the greatest chance for convective dominance owing to the likelihood of the juxtaposition of an upper-level trough and surface cold front sweeping through an unstable warm sector. Typical upper-level patterns associated with precipitation in the GL consist of a trough positioned upstream of the region along the Rocky Mountains. A downstream ridge would build over the NE, allowing for the trough to remain in place and continuous DCVA over the region. This pattern is consistent with the findings of Jennrich et al. (2020) in that there is a trough-ridge pattern in the GL that is favorable for precipitation. In fact, Fig. 3c in Jennrich et al. (2020) shows that both the trough upstream and the ridge downstream of the GL is statistically significant for these extreme precipitation events. At 850 hPa, a deepening cyclone is typically located along the NP and vicinity. Upstream of the cyclone, warm, moist air is advected into the region. As the cyclone moves over the region, a CFA along the western periphery of the cyclone moves over the warm, moist environment and creates additional lift for widespread precipitation. At the surface, there are 3 distinct patterns associated with the cyclone that help aid in

precipitation development (see Section 3.2.4). Each of these surface patterns involve a cold frontal passage through the region, which increases the likelihood of stratiform precipitation from large-scale ascent.

In the NE, all 5 of the events were characterized as mid-latitude environments and were strongly dominated by stratiform. There appears to be no seasonality in complete convective dominance (i.e., convective dominance greater than 50%), but there is seasonality in when convective precipitation is most likely to be expected (i.e., late spring to early summer). This, in part, is mostly due to the seasonality in surface temperature and available moisture in the region. The primary upper-level feature associated with these events was a longwave trough positioned just upstream of the region. This upper-level pattern promotes southerly moisture advection and strong QG forcing over the NE (Agel et al., 2019; Jennrich et al., 2020). At 850 hPa, a cyclone upstream of the region would promote southerly, Atlantic moisture into the region. One event that had a different pattern at 850 hPa was NE20110226. In this event, a deepening cyclone was over the region and a trowal was responsible for precipitation along the backside (upstream) of the cyclone. At the surface, there was a deepening cyclone with WAA ahead of the cyclone and a cold front with associated CAA behind the cyclone. Dowdy and Catto (2017) found that a cyclone with a frontal boundary is the most common cause of extreme precipitation in the NE. Catto and Pfahl (2013) found that roughly 40-50% of extreme precipitation (6-h ERA-Interim) in the NE occurs with warm fronts in close proximity to the precipitation.

Overall, tropical environments are confined to the lower latitude regions (i.e., SP and SE), and are more likely to occur in the summer months when temperatures are warm and moisture is easily accessible from the Gulf of Mexico. The poleward shift of the STJ in the summer months significantly reduces the dynamical forcing aloft. In turn, these events rely on mesoscale boundaries at the surface to provide the necessary lift to support precipitation and because of this, are predominately convective

in nature. Microphysically, these tropical environments are undergoing warm-rain processes, where particles mainly grow in the liquid phase at altitudes where temperatures are above 0°C. Mid-latitude environments were predominately stratiform dominant, and were not bound to any seasonality. Stratiform dominant precipitation east of the Rocky Mountains is primarily focused more poleward primarily because of the collocation of upper-level forcing and attendant synoptic boundaries at the surface. A few cases in the GL and one case in the NP were convectively dominant, but still held characteristics to mid-latitude environments (i.e., upper-level disturbances, synoptic boundaries, etc.). Mid-latitude environments are typically associated with cool rain processes where particles generally grow in the ice phase. Understanding the different environmental characteristics within each region will shed light on the microphyisical aspects of each precipitating event.

General synoptic patterns associated with extreme precipitation events throughout the CONUS include a trough/ridge dipole, with the trough axis centered just upstream of the region. This finding compliments the work done in Jennrich et al. (2020), where they found a trough/ridge dipole across many regions in the CONUS. Additionally, low-level moisture advection prior to and during the extreme precipitation event is similar to that in Jennrich et al. (2020). For most of the regions, the moisture source came from the Gulf of Mexico. In regions like the NP and GL, moisture could have come from the Gulf of Mexico, but it is more likely that low-level moisture advected into the region was recycled moisture from the SP or the SE. Many characteristic patterns associated with these extreme precipitation events found in this study agree with previous literature. This study is also consistent with Konrad (2001), who found that the position of the 500 hPa trough is upstream of the precipitating area. Additionally, Konrad (2001) suggested that there are characteristic patterns other than mid-level troughing that support extreme precipitation, such as moisture advection.

The results herein could be useful for the stakeholder communities east of the Rockies. Knowing the precipitation source for each region and seasonality can shed light on the daily impacts within an S2S extreme precipitation event. For example, if convective precipitation is more likely to occur during the summer in the SP, stakeholder communities within this region can expect more flash flooding with any training convective cells. From a predictability standpoint, these results are not intended to predict the S2S event itself, but rather the precipitation days within the S2S event. This information will be used to help build a statistical model in order to better predict these S2S extreme precipitation events, as apart of the broader PRES^{2}iP project.

One of the caveats that arise in this study is the dataset resolution. For example, it would be more advantageous to use a higher spatial and temporal resolution dataset in order to bolster greater confidence in convective/stratiform designation. Furthermore, increasing sensitivity to microphysics of precipitating systems, such that variability in radar-rain rate relations to tropical or mid-latitude designations can be accounted for. A limitation to the way this study utilizes PWAT is that a regional extrema threshold is based off of individual locations within the region. In addition, there is no classification algorithm that is perfect and it is possible that improvements to SL3D (or an alternative approach) could result in improvements of partitioning rainfall into convective and stratiform sources, but this is a minor source of variability in the long list of methods employed here. In the future, work could be done on additional metrics for characterizing mid-latitude/tropical environments (i.e., using tropopause height). In addition, future work could also include comparing environmental characteristics among regions and with greater statistical evaluation, rather than comparing event to event within the same region. With this additional knowledge, a statistical model could be built to help better predict these events. Finally, literature on extreme precipitation events in the GL and NP is lacking, so focusing on these two regions

specifically could help paint a better overall picture of extreme precipitation in the CONUS.

Bibliography

Agel, L., M. Barlow, F. Colby, H. Binder, J. L. Catto, A. Hoell, and J. Cohen, 2019: Dynamical analysis of extreme precipitation in the US northeast based on large-scale meteorological patterns. *Climate Dynamics*, **52**, 1739–1760, doi:10.1007/s00382-018-4223-2.

Ahern, M., R. S. Kovats, P. Wilkinson, R. Few, and F. Matthies, 2005: Global Health Impacts of Floods: Epidemiologic Evidence. *Epidemiologic Reviews*, **27 (1)**, 36–46, doi:10.1093/epirev/mxi004.

Alexander, L. V., et al., 2006: Global observed changes in daily climate extremes of temperature and precipitation. *Journal of Geophysical Research: Atmospheres*, **111 (D5)**, doi:10.1029/2005JD006290.

American Meteorological Society, 2017: Flash flood. American Meteorological Society, `http://glossary.ametsoc.org/wiki/Flash_flood`.

Anagnostou, E. N., 2004: A convective/stratiform precipitation classification algorithm for volume scanning weather radar observations. *Meteorological Applications*, **11 (4)**, 291–300, doi:10.1017/S1350482704001409.

Ashley, S. T. and W. S. Ashley, 2008: Flood fatalities in the united states. *Journal of Applied Meteorology and Climatology*, **47 (3)**, 805–818, doi:10.1175/2007JAMC1611.1.

Atlas, D. and C. Ulbrich, 2006: Drop size spectra and integral remote sensing parameters in the transition from convective to stratiform rain. *Geophysical Research Letters*, **33 (16)**, doi:10.1029/2006GL026824.

Austin, P. M., 1987: Relation between measured radar reflectivity and surface rainfall. *Monthly Weather Review*, **115 (5)**, 1053–1070, doi:10.1175/1520-0493(1987)115⟨1053:RBMRRA⟩2.0.CO;2.

Barlow, M., et al., 2019: North American extreme precipitation events and related large-scale meteorological patterns: a review of statistical methods, dynamics, modeling, and trends. *Climate Dynamics*, **53**, 6835–6875, doi:10.1007/s00382-019-04958-z.

Battan, L. J., 1973: Radar observation of the atmosphere.(the university of chicago press) 1973. pp x, 324; 125 figures, 21 tables. £7·15. **99 (422)**, 793–793, doi:10.1002/qj.49709942229.

Biggerstaff, M. I. and S. A. Listemaa, 2000: An Improved Scheme for Convective/Stratiform Echo Classification Using Radar Reflectivity. *Journal of Applied Meteorology*, **39 (12)**, 2129–2150, doi:10.1175/1520-0450(2001)040⟨2129:AISFCS⟩2.0.CO;2.

Bluestein, H. B., 1992: *Synoptic-Dynamic Meteorology in Midlatitudes*, Vol. 1. Oxford University Press, 338-343 pp.

Bluestein, H. B., 1993: *Synoptic-Dynamic Meteorology in Midlatitudes*, Vol. 2. Oxford University Press, 397-399 pp.

Bradley, A. A. and J. A. Smith, 1994: The Hydrometeorological Environment of Extreme Rainstorms in the Southern Plains of the United States. *Journal of Applied Meteorology*, **33 (12)**, 1418–1431, doi:10.1175/1520-0450(1994)033⟨1418:THEOER⟩2.0.CO;2.

Brooks, H. E. and D. J. Stensrud, 2000: Climatology of heavy rain events in the united states from hourly precipitation observations. *Monthly Weather Review*, **128 (4)**, 1194–1201, doi:10.1175/1520-0493(2000)128⟨1194:COHREI⟩2.0.CO;2.

Catto, J. L. and S. Pfahl, 2013: The importance of fronts for extreme precipitation. *Journal of Geophysical Research: Atmospheres*, **118 (19)**, 10,791–10,801, doi:10.1002/jgrd.50852.

Chandrasekar, V., E. Gorgucci, and G. Scarchilli, 1993: Optimization of multiparameter radar estimates of rainfall. *Journal of Applied Meteorology*, **32 (7)**, 1288–1293, doi:10.1175/1520-0450(1993)032⟨1288:OOMREO⟩2.0.CO;2.

Chen, G., et al., 2019: Microphysical characteristics of three convective events with intense rainfall observed by polarimetric radar and disdrometer in eastern china. doi:10.3390/rs11172004.

Coumou, D. and S. Rahmstorf, 2012: A decade of weather extremes. *Nature Climate Change*, **2**, 491–496, doi:https://doi.org/10.1038/nclimate1452.

Crum, T. D. and R. L. Alberty, 1993: The wsr-88d and the wsr-88d operational support facility. *Bulletin of the American Meteorological Society*, **74 (9)**, 1669–1688, doi:10.1175/1520-0477(1993)074⟨1669:TWATWO⟩2.0.CO;2.

Cunha, L. K., J. A. Smith, M. L. Baeck, and W. F. Krajewski, 2013: An Early Performance Evaluation of the NEXRAD Dual-Polarization Radar Rainfall Estimates for Urban Flood Applications. *Weather and Forecasting*, **28 (6)**, 1478–1497, doi:10.1175/WAF-D-13-00046.1.

Daly, C., G. H. Taylor, W. P. Gibson, T. W. Parzybok, G. L. Johnson, and P. A. Pasteris, 2000: High-quality spatial climate data sets for the united states and beyond. *Transactions of the ASAE*, **43 (6)**, 1957–1962, doi:10.13031/2013.3101.

Dougherty, E. and K. L. Rasmussen, 2019: Climatology of flood-producing storms and their associated rainfall characteristics in the united states. *Monthly Weather Review*, **147 (11)**, 3861–3877, doi:10.1175/MWR-D-19-0020.1.

Dowdy, A. J. and J. L. Catto, 2017: Extreme weather caused by concurrent cyclone, front and thunderstorm occurrences. *Scientific Reports*, **7**, doi:10.1038/srep40359.

Feng, Z., X. Dong, B. Xi, C. Schumacher, P. Minnis, and M. Khaiyer, 2011: Top-of-atmosphere radiation budget of convective core/stratiform rain and anvil clouds from deep convective systems. *Journal of Geophysical Research: Atmospheres*, **116 (D23)**, doi:10.1029/2011JD016451.

Flanagan, P. X., J. B. Basara, J. C. Furtado, and X. Xiao, 2018: Primary atmospheric drivers of pluvial years in the united states great plains. *Journal of Hydrometeorology*, **19 (4)**, 643–658, doi:10.1175/JHM-D-17-0148.1.

Funk, T., 2006: Heavy convective rainfall forecasting: Heavy convective rainfall forecasting: A comprehensive look at a comprehensive look at parameters, processes, patterns, and parameters, processes, patterns, and rules of thumb rules of thumb.

Gelaro, R., et al., 2017: The Modern-Era Retrospective Analysis for Research and Applications, Version 2 (MERRA-2). *Journal of Climate*, **30 (14)**, 5419–5454, doi:10.1175/JCLI-D-16-0758.1.

Giangrande, S. E. and A. V. Ryzhkov, 2008: Estimation of rainfall based on the results of polarimetric echo classification. *Journal of Applied Meteorology and Climatology*, **47 (9)**, 2445–2462, doi:10.1175/2008JAMC1753.1.

Gourley, J. J. and C. M. Calvert, 2003: Automated Detection of the Bright Band Using WSR-88D Data. *Weather and Forecasting*, **18 (4)**, 585–599, doi:10.1175/1520-0434(2003)018⟨0585:ADOTBB⟩2.0.CO;2.

Grams, H. M., J. Zhang, and K. L. Elmore, 2014: Automated Identification of Enhanced Rainfall Rates Using the Near-Storm Environment for Radar Precipitation Estimates. *Journal of Hydrometeorology*, **15 (3)**, 1238–1254, doi:10.1175/JHM-D-13-042.1.

Han, M., R. M. Rauber, M. K. Ramamurthy, B. F. Jewett, and J. A. Grim, 2007: Mesoscale Dynamics of the Trowal and Warm-Frontal Regions of Two Continental Winter Cyclones. *Monthly Weather Review*, **135 (5)**, 1647–1670, doi:10.1175/MWR3377.1.

Hasan, M. M., A. Sharma, F. Johnson, G. Mariethoz, and A. Seed, 2014: Correcting bias in radar z–r relationships due to uncertainty in point rain gauge networks. *Journal of Hydrology*, **519**, 1668 – 1676, doi:https://doi.org/10.1016/j.jhydrol.2014.09.060.

Hitchens, N. M., M. E. Baldwin, and R. J. Trapp, 2012: An object-oriented characterization of extreme precipitation-producing convective systems in the midwestern united states. *Monthly Weather Review*, **140 (4)**, 1356–1366, doi:10.1175/MWR-D-11-00153.1.

Houghton, H. G., 1968: On precipitation mechanisms and their artificial modification. *Journal of Applied Meteorology*, **7 (5)**, 851–859, doi:10.1175/1520-0450(1968)007⟨0851:OPMATA⟩2.0.CO;2.

Houze, R. A., Jr., 1982: Cloud clusters and large-scale vertical motions in the tropics. *Journal of the Meteorological Society of Japan. Ser. II*, **60 (1)**, 396–410, doi:10.2151/jmsj1965.60.1_396.

Houze, R. A., Jr., 1989: Observed structure of mesoscale convective systems and implications for large-scale heating. *Quarterly Journal of the Royal Meteorological Society*, **115 (487)**, 425–461, doi:10.1002/qj.49711548702.

Jennrich, G. C., J. C. Furtado, J. B. Basara, and E. R. Martin, 2020: Synoptic characteristics of 14-day extreme precipitation events across the united states. *Journal of Climate*, **0 (0)**, null, doi:10.1175/JCLI-D-19-0563.1.

Johnson, R. H., 1984: Partitioning tropical heat and moisture budgets into cumulus and mesoscale components: Implications for cumulus parameterization. *Monthly Weather Review*, **112 (8)**, 1590–1601, doi:10.1175/1520-0493(1984)112⟨1590:PTHAMB⟩2.0.CO;2.

Keim, B., 1996: Spatial, synoptic, and seasonal patterns of heavy rainfall in the southeastern united states. *Physical Geography*, **17**, 313–328.

Kirsch, B., M. Clemens, and F. Ament, 2019: Stratiform and convective radar reflectivity–rain rate relationships and their potential to improve radar rainfall estimates. *Journal of Applied Meteorology and Climatology*, **58 (10)**, 2259–2271, doi:10.1175/JAMC-D-19-0077.1.

Konrad, C. E., 1997: Synoptic-scale features associated with warm season heavy rainfall over the interior southeastern united states. *Weather and Forecasting*, **12 (3)**, 557–571, doi:10.1175/1520-0434(1997)012⟨0557:SSFAWW⟩2.0.CO;2.

Konrad, C. E., 2001: The most extreme precipitation events over the eastern united states from 1950 to 1996: Considerations of scale. *Journal of Hydrometeorology*, **2 (3)**, 309 – 325, doi:10.1175/1525-7541(2001)002⟨0309:TMEPEO⟩2.0.CO;2, URL `https://journals.ametsoc.org/view/journals/hydr/2/3/1525-7541_2001_002_0309_tmepeo_2_0_co_2.xml`.

Kunkel, K. E., T. R. Karl, D. R. Easterling, K. Redmond, J. Young, X. Yin, and P. Hennon, 2013: Probable maximum precipitation and climate change. *Geophysical Research Letters*, **40 (7)**, 1402–1408, doi:10.1002/grl.50334.

Maddox, R. A., C. F. Chappell, and L. R. Hoxit, 1979: Synoptic and meso-α scale aspects of flash flood events. *Bulletin of the American Meteorological Society*, **60 (2)**, 115–123, doi:10.1175/1520-0477-60.2.115.

Marciano, C. G. and G. M. Lackmann, 2017: The south carolina flood of october 2015: Moisture transport analysis and the role of hurricane joaquin. *Journal of Hydrometeorology*, **18 (11)**, 2973–2990, doi:10.1175/JHM-D-16-0235.1.

Marshall, J. S. and W. M. K. Palmer, 1948: The distribution of raindrops with size. *Journal of Meteorology*, **5 (4)**, 165–166, doi:10.1175/1520-0469(1948)005⟨0165:TDORWS⟩2.0.CO;2.

Meehl, G. A., et al., 2007: Global climate projections.

Min, S.-K., X. Zhang, F. Zwiers, and G. Hegerl, 2011: Human contribution to more-intense precipitation extremes. *Nature*, **470**, 378–381, doi:https://doi.org/10.1038/nature09763.

Moore, B. J., K. M. Mahoney, E. M. Sukovich, R. Cifelli, and T. M. Hamill, 2015: Climatology and environmental characteristics of extreme precipitation events in the southeastern united states. *Monthly Weather Review*, **143 (3)**, 718–741, doi:10.1175/MWR-D-14-00065.1.

Moore, B. J., P. J. Neiman, F. M. Ralph, and F. E. Barthold, 2012: Physical processes associated with heavy flooding rainfall in nashville, tennessee, and vicinity during 1–2 may 2010: The role of an atmospheric river and mesoscale convective systems. *Monthly Weather Review*, **140 (2)**, 358–378, doi:10.1175/MWR-D-11-00126.1.

Morrison, H., G. Thompson, and V. Tatarskii, 2009: Impact of cloud microphysics on the development of trailing stratiform precipitation in a simulated squall line: Comparison of one- and two-moment schemes. *Monthly Weather Review*, **137 (3)**, 991–1007, doi:10.1175/2008MWR2556.1.

National Weather Service, 1997: The flood of march 1997. National Oceanic and Atmospheric Administration, `https://www.weather.gov/lmk/flood97`.

National Weather Service, 2013: September 2013 floods. National Oceanic and Atmospheric Administration, `https://www.weather.gov/bou/Number1September2013Floods`.

National Weather Service, 2017: Noaa next generation radar (nexrad) level 3 products. National Oceanic and Atmospheric Administration, `https://data.noaa.gov/dataset/dataset/noaa-next-generation-radar-nexrad-level-3-products`.

National Weather Service, 2018a: Summary of natural hazard statistics for 2018 in the united states. National Oceanic and Atmospheric Administration, `https://www.weather.gov/media/hazstat/sum18.pdf`.

National Weather Service, 2018b: Weather related fatality and injury statistics. National Oceanic and Atmospheric Administration, `https://www.weather.gov/hazstat/`.

Powell, S. W., J. Houze, Robert A., and S. R. Brodzik, 2016: Rainfall-Type Categorization of Radar Echoes Using Polar Coordinate Reflectivity Data. *Journal of Atmospheric and Oceanic Technology*, **33 (3)**, 523–538, doi:10.1175/JTECH-D-15-0135.1.

PRISM Climate Group, ????: PRISM Climate Group, http://prism.oregonstate.edu, created 18 SEP 2020, http://prism.oregonstate.edu, created 18 SEP 2020.

Ross, R. J. and W. P. Elliott, 1996: Tropospheric Water Vapor Climatology and Trends over North America: 1973–93. *Journal of Climate*, **9 (12)**, 3561–3574, doi:10.1175/1520-0442(1996)009⟨3561:TWVCAT⟩2.0.CO;2.

Ryzhkov, A., M. Diederich, P. Zhang, and C. Simmer, 2014: Potential utilization of specific attenuation for rainfall estimation, mitigation of partial beam blockage, and radar networking. *Journal of Atmospheric and Oceanic Technology*, **31 (3)**, 599–619, doi:10.1175/JTECH-D-13-00038.1.

Ryzhkov, A. V., S. E. Giangrande, and T. J. Schuur, 2005: Rainfall estimation with a polarimetric prototype of wsr-88d. *Journal of Applied Meteorology*, **44 (4)**, 502–515, doi:10.1175/JAM2213.1.

Schroeder, A., J. Basara, J. M. Shepherd, and S. Nelson, 2016: Insights into atmospheric contributors to urban flash flooding across the united states using an analysis of rawinsonde data and associated calculated parameters. *Journal of Applied Meteorology and Climatology*, **55 (2)**, 313–323, doi:10.1175/JAMC-D-14-0232.1.

Schubert, S. D., M. J. Suarez, P. J. Pegion, R. D. Koster, and J. T. Bacmeister, 2008: Potential predictability of long-term drought and pluvial conditions in the u.s. great plains. *Journal of Climate*, **21 (4)**, 802–816, doi:10.1175/2007JCLI1741.1.

Schumacher, C. and R. A. Houze, 2003: Stratiform rain in the tropics as seen by the trmm precipitation radar. *Journal of Climate*, **16 (11)**, 1739–1756, doi:10.1175/1520-0442(2003)016⟨1739:SRITTA⟩2.0.CO;2.

Schumacher, R. S. and R. H. Johnson, 2006: Characteristics of u.s. extreme rain events during 1999–2003. *Weather and Forecasting*, **21 (1)**, 69–85, doi:10.1175/WAF900.1.

Seed, A. W., J. Nicol, G. L. Austin, C. D. Stow, and S. G. Bradley, 2007: The impact of radar and raingauge sampling errors when calibrating a weather radar. *Meteorological Applications*, **3 (1)**, 43–52, doi:10.1002/met.5060030105.

Sillmann, J., V. V. Kharin, F. W. Zwiers, X. Zhang, and D. Bronaugh, 2013: Climate extremes indices in the cmip5 multimodel ensemble: Part 2. future climate projections. *Journal of Geophysical Research: Atmospheres*, **118 (6)**, 2473–2493, doi:10.1002/jgrd.50188.

Smith, J. A., M. L. Baeck, J. E. Morrison, and P. Sturdevant-Rees, 2000: Catastrophic Rainfall and Flooding in Texas. *Journal of Hydrometeorology*, **1 (1)**, 5–25, doi: 10.1175/1525-7541(2000)001⟨0005:CRAFIT⟩2.0.CO;2.

Smith, J. A., M. L. Baeck, G. Villarini, and W. F. Krajewski, 2010: The Hydrology and Hydrometeorology of Flooding in the Delaware River Basin. *Journal of Hydrometeorology*, **11 (4)**, 841–859, doi:10.1175/2010JHM1236.1.

Smith, J. A., D. J. Seo, M. L. Baeck, and M. D. Hudlow, 1996: An intercomparison study of nexrad precipitation estimates. *Water Resources Research*, **32 (7)**, 2035–2045, doi:10.1029/96WR00270.

Smith, W. and R. J. Younkin, 1972: An Operationally Useful Relationship Between the Polar Jet Stream and Heavy Precipitation. *Monthly Weather Review*, **100**, 434–440.

Starzec, M., C. R. Homeyer, and G. L. Mullendore, 2017: Storm Labeling in Three Dimensions (SL3D): A Volumetric Radar Echo and Dual-Polarization Updraft Classification Algorithm. *Monthly Weather Review*, **145 (3)**, 1127–1145, doi: 10.1175/MWR-D-16-0089.1.

Steiner, M. and R. A. Houze, 1997: Sensitivity of the estimated monthly convective rain fraction to the choice of z–r relation. *Journal of Applied Meteorology*, **36 (5)**, 452–462, doi:10.1175/1520-0450(1997)036⟨0452:SOTEMC⟩2.0.CO;2.

Steiner, M., R. A. Houze, and S. E. Yuter, 1995: Climatological characterization of three-dimensional storm structure from operational radar and rain gauge data. *Journal of Applied Meteorology*, **34 (9)**, 1978–2007, doi:10.1175/1520-0450(1995)034⟨1978:CCOTDS⟩2.0.CO;2.

Stevenson, S. N. and R. S. Schumacher, 2014: A 10-year survey of extreme rainfall events in the central and eastern united states using gridded multisensor precipitation analyses. *Monthly Weather Review*, **142 (9)**, 3147–3162, doi: 10.1175/MWR-D-13-00345.1.

Storm Prediction Center (SPC), ????: Storm prediction center sounding climatology page. National Oceanic and Atmospheric Administration, `https://www.spc.noaa.gov/exper/soundingclimo/`.

Tao, W.-K., S. Lang, X. Zeng, S. Shige, and Y. Takayabu, 2010: Relating convective and stratiform rain to latent heating. *Journal of Climate*, **23 (7)**, 1874–1893, doi: 10.1175/2009JCLI3278.1.

Trenberth, K. E., A. Dai, R. M. Rasmussen, and D. B. Parsons, 2003: The Changing Character of Precipitation. *Bulletin of the American Meteorological Society*, **84 (9)**, 1205–1218, doi:10.1175/BAMS-84-9-1205.

Villarini, G. and W. Krajewski, 2010: Review of the different sources of uncertainty in single polarization radar-based estimates of rainfall. *Surveys in Geophysics*, **31 (1)**, 107–129, doi:https://doi.org/10.1007/s10712-009-9079-x.

Warning Decision Training Division (WDTD), 2014: Surface precipitation rate (spr). National Oceanic and Atmospheric Administration, `https://vlab.ncep.noaa.gov/web/wdtd/-/surface-precipitation-rate-sp-3`.

Weather Prediction Center, 2020: National Oceanic and Atmospheric Administration, `https://www.wpc.ncep.noaa.gov/archives/web_pages/sfc/sfc_archive.php`.

Westra, S., et al., 2014: Future changes to the intensity and frequency of short-duration extreme rainfall. *Reviews of Geophysics*, **52 (3)**, 522–555, doi:10.1002/2014RG000464.

Westrick, K. J., C. F. Mass, and B. A. Colle, 1999: The Limitations of the WSR-88D Radar Network for Quantitative Precipitation Measurement over the Coastal Western United States. *Bulletin of the American Meteorological Society*, **80 (11)**, 2289–2298, doi:10.1175/1520-0477(1999)080⟨2289:TLOTWR⟩2.0.CO;2.

Yang, Z., P. Liu, and Y. Yang, 2019: Convective/stratiform precipitation classification using ground-based doppler radar data based on the k-nearest neighbor algorithm. *Remote Sensing*, **11**, 2277, doi:10.3390/rs11192277.